ENHANCEMENT OF POOL BOILING HEAT TRANSFER IN CONFINED SPACE

A Thesis

by

CHIA-HSIANG HSU

Submitted to the Office of Graduate and Professional Studies of
Texas A&M University
in partial fulfillment of the requirements for the degree of

MASTER OF SCIENCE

Chair of Committee,	Jorge L. Alvarado
Committee Members,	Yassin A. Hassan
	Debjyoti Banerjee
Head of Department,	Andreas A. Polycarpou

May 2014

Major Subject: Mechanical Engineering

ABSTRACT

Pool boiling is an effective method used in many technical applications for a long time. Its highly efficient heat transfer performance results from not only the convection effect but also the phase change process in pool boiling. Pool boiling enhancement has been studied in the past decade. However, the mechanisms of pool boiling has not yet been fully understood because of the many parameters that affect its behavior including the latent heat of vaporization, nucleation density, bubble and fluid motion, interaction at the interface, and the physical properties of surface. Among the current studies, bubble departure rate is viewed as one of the dominant factors that affect heat transfer.

This research considers the effect of bubble confinement on pool boiling. In the study, confinement was achieved by placing a flat plate over heated surface. The flat plate has a hole in the middle, and there is a gap between the flat plate and the heater. The diameters of hole are 2 mm, 3 mm, and 4 mm; the gap distances are 2.3 mm, 3.6 mm, and 5 mm. The heater consists of an indium-tin-oxide layer deposited on a silicon wafer. An IR camera and high speed cameras are used to acquire the surface temperature distribution and bubble image. By controlling the plate hole size and the gap distance, the effect of confinement on heat transfer performance can be evaluated. Moreover, heat transfer performance of pool boiling with three-2mm-holes plate was investigated and compared with that of single-2mm-hole plate with the smallest gap size.

At the lower heat flux values, heat transfer enhancement in confined space was experimentally observed. Surface temperature can be reduced by 4 **℃** at most. Results

indicate that higher bubble departure rate and coalescence effect might be the dominant factor for improving heat transfer performance in a confined space caused by induced shear flow.

DEDICATION

To Dr. Jorge L. Alvarado for his inspiration and support

To my family for their unconditional love

ACKNOWLEDGEMENTS

I would like to thank my committee chair, Dr. Alvarado, and my committee members, Dr. Hassan and Prof. Banerjee, for their guidance and support throughout the course of this research.

Thanks also go to my friends and colleagues and the department faculty and staff for making my time at Texas A&M University a great experience.

Finally, thanks to my mother and father for their encouragement.

NOMENCLATURE

c_{pl}	liquid specific heat
f	bubble frequency
g	gravitational acceleration
h_{fg}	latent heat of vaporization per unit mass
k_l	thermal conductivity of liquid
$n_a{}'$	density of active nucleation sites on the surface
Pr_l	liquid Prandtl number
q''	heat flux
R_{max}	maximum bubble radius
R_0	threshold radius
T_{sat}	liquid saturated temperature
T_w	wall temperature
μ_l	liquid viscosity
ρ_l	liquid density
ρ_v	vapor density
σ	interfacial tension

TABLE OF CONTENTS

Page

ABSTRACT ii

DEDICATION iv

ACKNOWLEDGEMENTS v

NOMENCLATURE vi

TABLE OF CONTENTS vii

LIST OF FIGURES ix

LIST OF TABLES xii

1. INTRODUCTION 1

1.1 Background & motivation 1
1.2 Objective 2

2. LITERATURE REVIEW 4

2.1 Fundamentals 4
2.1.1 Boiling curve 4
2.1.2 Rohsenow's model 7
2.1.3 Vapor-liquid exchange model 7
2.2 Enhancement of pool boiling heat transfer review 9
2.2.1 Surface modification 9
2.2.1.1 Surface characteristics 9
2.2.1.2 Particles and pores 11
2.2.1.3 Structure 13
2.2.2 Additives for fluid 14
2.2.3 Use of heat transfer enhancers 16

3. EXPERIMENT FACILITIES AND METHODS 19

3.1 Experiment facilities 19
3.1.1 Working fluid 20
3.1.2 Test chamber 21
3.1.3 Heating element 25

3.1.4 Data acquisition system 27
3.1.4.1 Infrared camera 27
3.1.4.2 High speed camera 29
3.1.5 Power supply 29
3.1.6 Chiller 30
3.2 Experimental method 30
3.2.1 Emissivity measurement 30
3.2.2 Heat loss estimation 32
3.2.3 Procedure 33
3.2.4 Uncertainty analysis 34

4. RESULTS AND DISCUSSION 36

4.1 Unconfined pool boiling 36
4.2 Effect of plate gap size on confined pool boiling phenomena 39
4.3 Effect of plate hole diameter on confined pool boiling 49
4.3.1 Analysis of pool boiling heat transfer performance by fluid and bubble behavior in confined spaces 52
4.3.2 Analysis of pool boiling heat transfer performance due to coalesced bubble departure frequency and diameter 55
4.4 Effect of the triple hole plate on confined pool boiling 62

5. CONCLUSION 67

REFERENCES 69

APPENDIX A 75

APPENDIX B 78

APPENDIX C 79

LIST OF FIGURES

Page

Figure 2.1 Boiling curve 6

Figure 2.2 Bubble Regimes 6

Figure 3.1 Scheme of pool boiling setup 19

Figure 3.2 Photo of pool boiling setup 20

Figure 3.3 Scheme of test chamber 22

Figure 3.4 Photo of test chamber 22

Figure 3.5 Design drawing of sample holder 23

Figure 3.6 3-D simulation of sample holder 24

Figure 3.7 Top view photo of confined space 24

Figure 3.8 Side view photo of confined space 25

Figure 3.9 Scheme of heating element setup 27

Figure 3.10 Infrared camera SC7650-MB with lens 28

Figure 3.11 High speed camera FASTCAM SA3 with lens 29

Figure 3.12 Emissivity value of heater at different temperatures 32

Figure 3.13 Calibration of heat loss corresponding to different temperature difference 33

Figure 4.1 Surface temperature map acquired using IR camera in unconfined pool boiling at 18 W/cm^2 38

Figure 4.2 Boiling curve of unconfined pool boiling 38

Figure 4.3 Bubble images of unconfined pool boiling at (a) 6 W/cm^2 (b) 15 W/cm^2 (c) 33 W/cm^2 39

Figure 4.4 Boiling curve of confined space with 2 mm hole plate, Case A – C 41

Figure 4.5 Boiling curve of confined space with 3 mm hole plate, Case D – F 42

Figure 4.6 Boiling curve of confined space with 3 mm hole plate, Case G – I 42

Figure 4.7 Bubble images in confined space with 2 mm hole plate, 5.75W/cm^2..... 44

Figure 4.8 Bubble images in confined space with 3 mm hole plate, 8W/cm^2..... 45

Figure 4.9 Bubble images in confined space with 4 mm hole plate, 9.5W/cm^2..... 46

Figure 4.10 IR images in the confined space when the coalesced bubble departs through the hole..... 48

Figure 4.11 Temporal surface temperature in the confined space when the coalesced bubble forms and departs..... 48

Figure 4.12 Boiling curve of confined space in 2.3 mm gap, case A, D and G..... 51

Figure 4.13 Percentage of enhancement in heat transfer coefficient as a function of heat flux, case A, D, and G..... 51

Figure 4.14 Percentage of enhancement in heat transfer coefficient as function of superheat (ΔT), case A, D and G..... 52

Figure 4.15 IR image of surface temperature field caused by the motion of fluid in the confined space for case D at a heat flux of 1.5 W/cm^2..... 53

Figure 4.16 Bubble image of confined space in 2.3 mm gap with different hole diameter, 4.2 W/cm^2..... 54

Figure 4.17 Bubble image of confined space in 2.3 mm gap with 4 mm hole diameter, 17W/cm^2..... 54

Figure 4.18 Departure frequency and diameter of the coalesced bubble as a function of heat flux in the confined space with 2 mm hole (case A)..... 57

Figure 4.19 Departure frequency and diameter of the coalesced bubble as a function of heat flux in the confined space with 3 mm hole (case D)..... 58

Figure 4.20 Departure frequency and diameter of the coalesced bubble as a function of ΔT in the confined space with 2 mm hole (case A)..... 59

Figure 4.21 Departure frequency and diameter of the coalesced bubble as a function of ΔT in the confined space with 3 mm hole (case D)..... 60

Figure 4.22 Comparison of the frequency times volume as a function of heat flux in the confined space with 2 mm and 3 mm hole..... 61

Figure 4.23 Comparison of the frequency times volume as a function of ΔT in the confined space with 2 mm and 3 mm hole 62

Figure 4.24 Boiling curve of the confined space with 2 mm hole and triple 2 mm holes and 2.3 mm gap 63

Figure 4.25 Percentage of enhancement in heat transfer coefficient as a function of heat flux 63

Figure 4.26 Percentage of enhancement in heat transfer coefficient as a function of superheat (ΔT) 64

Figure 4.27 Bubble image of the confined space with triple 2 mm hole plate in 2.3 mm gap, 15 W/cm^2 65

Figure 4.28 Bubble image of the confined space with 2 mm hole and triple 2 mm hole plate in 2.3 mm gap, 3 W/cm^2 66

Figure C.1 Boiling curve with error bar of confined space with 2 mm hole plate, Case A – C 79

Figure C.2 Boiling curve with error bar of confined space with 3 mm hole plate, Case D – F 79

LIST OF TABLES

Page

Table 3.1 HFE-7100 properties 21

Table 3.2 Properties of silicon wafer 27

Table 4.1 Cases table 40

Table 4.2 Effects of gap and hole size on confined pool boiling performance 43

Table 4.3 Departure frequency and diameter of confined space with 2 mm and 3 mm hole in the different value of heat flux 57

Table 4.4 Departure frequency and diameter of coalesced bubble in confined space with 2 mm and 3 mm hole 59

1. INTRODUCTION

1.1 Background & motivation

The liquid-vapor phase change process has been used in technological application for a long time. Boiling and condensation are well-known phase change processes and have been investigated for many years. Boiling is the process where liquid absorbs heat from the surface of the heating element and then it changes to vapor. Inversely, condensation is the process where vapor dissipates heat to the surface of a cold object and then is converted to liquid. Phase change process plays a very important role in these processes because a large amount of heat can be released and absorbed by the surface quickly, even if there is only a slight temperature difference between surface and fluid. This efficient heat transfer performance has continued to attract research groups to dedicate themselves to the study of the two-phase change process.

Pool boiling is a specific type of boiling where evaporation occurs in the quiescent liquid, allowing flow arising from free convection and bubble motion. Pool boiling is also characterized into two types: sub-cooled and saturated. Sub-cooled pool boiling happens when working fluid operates below the liquid saturated temperature and bubbles formed at the surface condense back to liquid. Saturated pool boiling occurs when working fluid keeps the temperature saturated and bubbles on the surface depart due to buoyant forces.

There is a long history of research in pool boiling. In 1934, Nukiyama [1] first investigated and obtained the saturated pool boiling curve, used to describe the pool boiling performance as a heat transfer mode. The curve was separated by several regimes and the behaviors in each regime were also described. Later, additional researchers postulated models to explain the behavior of pool boiling based on simple assumptions. The mechanisms of pool boiling, however, are not yet fully understood. The study of pool boiling mechanisms has been challenging because of the many parameters that are used to describe pool boiling including latent heat of vaporization, density of nucleation sites, bubble and fluid motion, solid-liquid interactions at the interface, and the physical properties of surfaces. Recently, due to the rapid development of electronic technology, devices with higher efficiency of heat transfer are becoming popular. Many research groups have investigated how to improve the performance of pool boiling. The results show that out of all of the parameters, the bubble departure rate is one of the dominant factors affecting the performance of heat transfer.

In this project, enhancement of pool boiling heat transfer was studied by creating and utilizing a confined space, which is used to improve shear flow and increase the bubble departure rate; therefore, increasing heat transfer in pool boiling.

1.2 Objective

The specific objective of this research was to study pool boiling heat transfer in a confined space, achieved by adding and utilizing a flat plate over a heated surface. The flat plate has a hole in the middle, and there is a gap between the plate and the heater

surface. An infrared camera and a high speed camera were used to acquire the surface temperature distribution and bubble images. By observing the pictures obtained from these cameras, while utilizing various hole sizes and gap distances, the effects of confined space were analyzed and discussed.

2. LITERATURE REVIEW

2.1 Fundamentals

Boiling is a process by which liquid absorbs the heat from a hot surface to change the liquid into vapor bubbles. Boiling occurs when the surface temperature is higher than the liquid's saturation temperature at a given pressure. Following are the concepts of the boiling curve and nucleate pool boiling models which are cited most widely.

2.1.1 Boiling curve

The boiling curve, a qualitative description of boiling performance, was first brought up by Nukiyama [1]. The curve, shown in Figure 2.1, shows the relationship between heat flux and the wall superheat, which means the temperature difference between surface and saturated liquid ($\Delta T=T_w-T_{sat}$). It is segmented into five regimes characterized by the nature of vapor formation: natural convection, isolated nucleate boiling, fully developed nucleate boiling, transition boiling, and film boiling. The schemes of each regime are shown in Figure 2.2.

In the first regime, when the surface temperature is increased slightly above the liquid saturated temperature, heat is transferred to the liquid by natural convection and finally it is dissipated out of the free surface via evaporation. As the surface temperature is increased, nucleate boiling occurs and vapor bubbles form on some separated nucleation sites. This regime is called isolated nucleate boiling and the initiation of

vapor bubble formation on the surface is designated the onset of nucleate boiling (ONB, point A). With increasing the surface temperature, more nucleation sites are initiated and bubble forming on different nucleate sites start to coalesce. This regime is called fully developed nucleate boiling. Eventually, the value of heat flux reaches a maximum value called critical heat flux (CHF, point C) because a vapor film begins to form on the surface and these dry portions of the surface start experiencing worse heat transfer performance. If the temperature increases continuously, more dry portions appear and the heat transfer coefficient decreases in this regime which is called transition boiling. Once the vapor film covers the whole surface, heat flux increases with increasing superheat. Radiation is also considered in this regime because its effects are important at the high wall temperature. This regime is called film boiling.

If the heat flux is increased, the boiling curve jumped from the point of the critical heat flux to the point E in the film boiling regime when the heat flux is higher than the critical heat flux. Conversely, in the process of decreasing heat flux from the film boiling regime, the temperature would sudden decrease once the supplied heat flux is under the minimum heat flux.

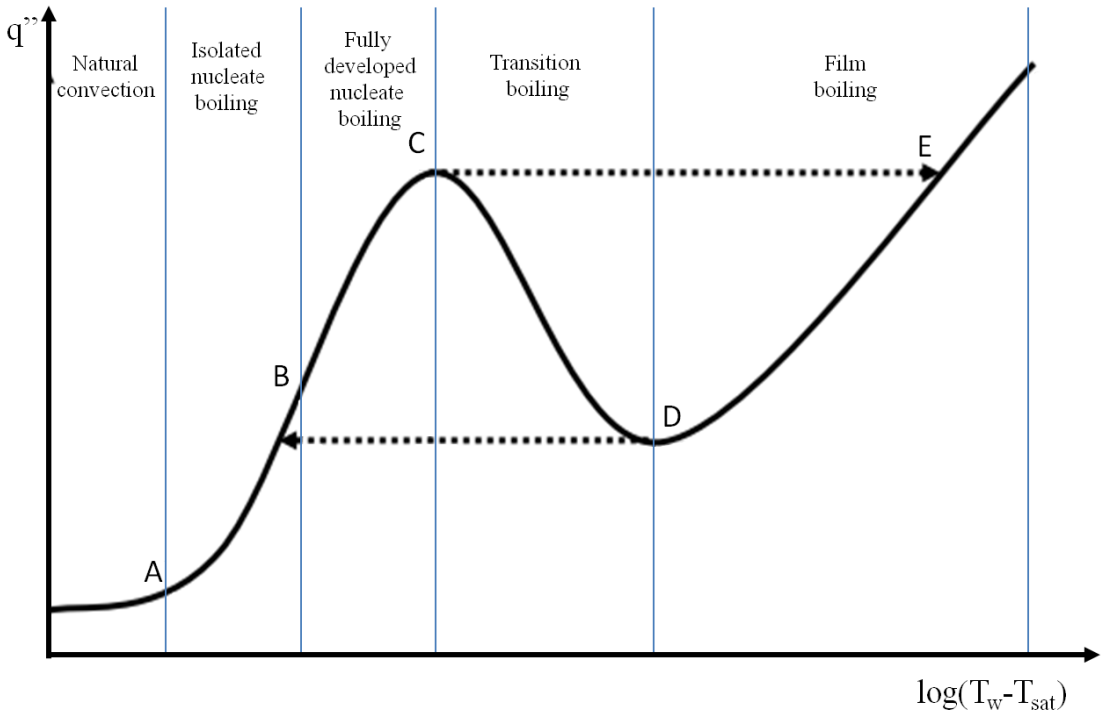

Figure 2.1 Boiling curve [1]

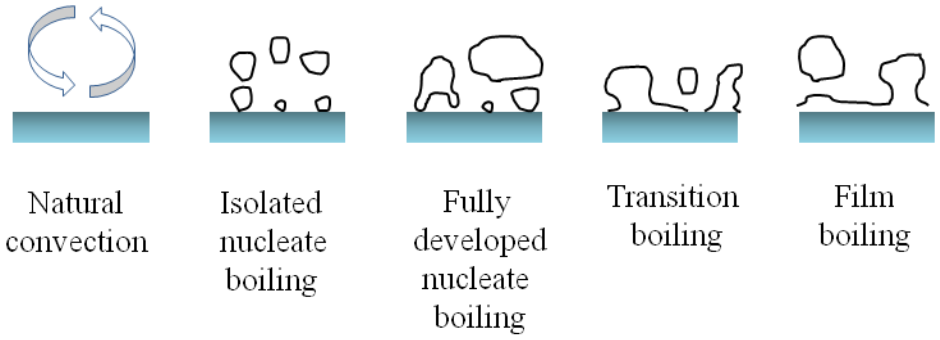

Figure 2.2 Bubble Regimes [2]

2.1.2 Rohsenow's model

The first and the most widely cited model in the past for pool boiling research is the Rohsenow's model. Rohsenow [3] assumed the heat transfer in the pool boiling as a single-phase convection process and the high heat transfer coefficient was due to the local liquid agitation caused by the motion of liquid flowing behind the wake of departing bubbles. By specifying the length and velocity into the single-phase forced convection heat transfer correlation, the correlation of pool boiling heat transfer could be determined. In Rohsenow's model, bubble departure diameter and vapor superficial velocity were used as the length and velocity scales, respectively. The correlation of nucleate pool boiling is given as follows:

$$q" = \mu_l h_{fg} \left[\frac{g(\rho_l - \rho_v)}{\sigma}\right]^{1/2} \left(\frac{c_{pl}\Delta T}{C_{sf} h_{fg} Pr_l^n}\right)^3 \tag{2.1}$$

where C_{sf} and n are the experimentally determined value for different liquid-solid combinations.

2.1.3 Vapor-liquid exchange model

Forster and Greif [4] proposed the vapor-liquid exchange mechanism that the forming bubble would push heated liquid out of near-wall region as the bubble grows; then, when the bubble departs from the surface, the cooler liquid would be drawn to the surface. They further assumed the volume of pushed by the liquid was equal to the

bubble departure volume. Based on the mechanistic bubble volume behavior, the following correlation was developed:

$$q" = \rho_l c_{pl} \left(\frac{2\pi}{3}\right) R_{max}^3 \left(\frac{1}{2}\right) (T_w - T_l) f n_a' \tag{2.2}$$

Based on the vapor-liquid exchange concept, Mikic and Rohsenow [5] derived a correlation for saturated pool boiling. The correlation states that heat is transferred from the surface by two mechanisms: natural convection between active nucleation sites and the liquid-vapor exchange phenomena at the active sites. The simple one-dimensional transient conduction process in a semi-infinite medium was used to model the transient conduction process that cooler liquid flowed to the surface after bubble departure. The mean surface heat flux can be expresses as follow:

$$\frac{\overline{q"}}{\mu_l h_{lv}} \left[\frac{\sigma}{g(\rho_l - \rho_v)}\right]^{1/2} = B[\emptyset (T_w - T_{sat})]^{m+1} \tag{2.3}$$

$$B = A_1^{3/2} A_2^{1/2} A_3 \left(\frac{2\pi^{1/2}}{g^{9/8}}\right) \left(\frac{R_0}{2}\right)^m$$

$$\emptyset = \left[\frac{k_l^{1/2} \rho_l^{17/8} c_{pl}^{19/8} h_{lv}^{m-23/8} \rho_v^{m-15/8}}{\mu_l (\rho_l - \rho_v)^{9/8} \sigma^{m-11/8} T_{sat}^{m-15/8}}\right]^{1/(m+1)}$$

where A_1 and A_2 are experimentally determined value for different liquid and A_3, R_0, and m are the values related to the active nucleation cites and cavity radius.

2.2 Enhancement of pool boiling heat transfer review

In the past, many studies had used several techniques to enhance the performance of pool boiling. Bergles [6] summarized that enhancement methods could be divided into passive, active and compound techniques. In passive techniques, three main techniques were categorized as surface modification, additives for fluid and the use of heat transfer enhancers. Below are the reviews investigated for these three techniques.

2.2.1 Surface modification

Generally enhancement by surface modification can be categorized in two ways: changing the surface characteristics macroscopically and using micro or nano features on the surface.

2.2.1.1 Surface characteristics

Roughness is commonly accepted as one of the most important parameters in surface characteristics for enhancing the heat transfer coefficient due to an increase in the number of nucleation sites. Berenson [7] investigated the effect of roughness on pool boiling heat transfer performance with n-pentane as working fluid. Several methods were used to improve surface finish and boiling curves were measured to compare the performance of pool boiling heat transfer of the different surfaces. The author concluded that the heat transfer coefficient could increase up by 600% by changing surface roughness but they also found that the critical heat flux was independent of surface roughness. However, surface roughness is not the only factor that affects the heat

transfer coefficient unless vapors could be trapped by the grooves associated with increased roughness [8]. Grigor'ev et al. [9] studied the heat transfer coefficient of boiling of cryogenic fluid with various surface roughness values. They concluded that there was no difference in the heat transfer coefficient between the cases with the surface roughness (R_z) of 5 and 10 µm, but heat transfer coefficient in the case with a surface roughness (R_z) of 1 µm was lower by a factor of 5 times than the two cases with greater roughness. The results showed that it is hard to evaluate the effect of surface roughness on heat transfer coefficient [10]. This is because the number of nucleation sites is not affected only by geometric size of the surface features but also by aging, surface chemistry, surface-liquid interactions and wettability. Furthermore, the surface features should be poorly wetted or steep walled to enhance the heat transfer coefficient [8].

Wettability was usually not considered as a promoter of heat transfer coefficient enhancement because of the vapor trapping capability of the cavities. When surface wettability increases, vapor bubbles are hard to be trapped which leads to higher superheats and higher surface temperatures. However, surface wettablility is an important factor in improving critical heat flux. Takata et al. [11] studied the effect of wettability on critical heat flux in pool boiling. A superhydrophilic surface made by exposing the TiO_2 coated surface with UV light was used in their research. The results indicate that critical heat flux of coated surface was about two times higher than non-coated surface because of an increased wettability.

The effects of heater size on pool boiling have also been studied for years. Many researchers have characterized the effects of heater size by using the capillary length (L_c), which is given by the following equation.

$$L_c = \sqrt{\frac{\sigma}{g(\rho_l - \rho_v)}} \tag{2.4}$$

Lu et al. [12] investigated the critical heat flux of pool boiling on the silicon array-coated surface with different sizes heater. They concluded that the critical heat flux increased when the heater size decreased, and the effect of heater size became significantly when the heater length is smaller than 8 times the capillary length. The similar results were also shown by Lienhard et al. [13] and Rainey and You [14]. They showed that the critical heat flux value decreased with the increase the heater size. Furthermore, Lienhard et al. attributed the behavior to the number of "vapor jets" which could be supported by the heater. However, for the heat transfer performance in the nucleate boiling regime, Park and Bergles [15] observed that the effect of heater size was insensitive.

2.2.1.2 Particles and pores

Deposition of metal particles on surfaces is also one method that could enhance the nucleate pool boiling heat transfer. Cieśliński [16] used different materials (Al, Cu, Mo, Zn, Brass, etc.) to coat a heater surface and investigated the influence of the porous coating on the heat transfer rate. The results showed that the metal coated surface had higher heat transfer coefficient than smooth surface at the same heat flux, and the

aluminum coated surface had better performance than other materials. He also concluded that the most relevant factor was the contact between the porous matrix and the substrate. O'Connor et al. [17] also used the "spraying" and "painting" methods to deposit the alumina and diamond particles on surfaces as the micro-porous structure to enhance the heat transfer performance. The painting surface resulted in up to 85% reduction for incipient superheat, 70-80% reduction in nucleate boiling superheat and as much as 100% increase in critical heat flux.

Recently, nano-techniques have been developed by extending and improving the techniques of microporous surface preparation. Vemuri and Kim [18] used a nano-porous surface with 70 μm thickness and 50-250 nm pores diameter in pool boiling experiments with FC-72. The incipient superheat for the nano-porous coated surface was reduced by about 30% as compared to the plain aluminum surface. Forrest et al. [19] developed nano-porous surfaces by the layer-by-layer assembly method to investigate the effects of surface properties on CHF and heat transfer coefficient augmentation. The surface was coated using nanoparticles layer by layer and the wetting properties changed depending on the final treatment. The heat transfer coefficient was enhanced by 100% and the critical heat flux was also enhanced by 44% when the surface was hydrophobic, characterized by static and advancing contact angles of 140° and 160°, and a much smaller receding contact angle of 20°. The enhancement of CHF indicates the importance of receding contact angle on critical heat flux. Tang et al. [20] studied pool boiling heat transfer performance by using a facile hot-dip galvanizing/dealloying (HDGD) process for the fabrication of nano-porous surface because the process was a good method for

fabricating metallic nano-porous surface with high thermal conductivity. The results indicate a 172% enhanced in the heat transfer coefficient and the thermal conductivity of nano-structure was found to be an important factor for enhancing boiling performance.

2.2.1.3 Structure

Fabrication of structure on pool boiling surfaces has also been considered as another effective method for improving boiling heat transfer performance. Guglielmini et al. [21] studied the pool boiling heat transfer performance when using finned copper surfaces. Two finned surfaces were used in their research. The results showed that heat transfer coefficients of the two finned surfaces were similar but much higher than the plain surface at the low superheat. Wei and Honda [22] also obtained similar results in terms of heat transfer performance. They considered the effects of fin thickness and fin height on micro-pin-fin heat transfer performance of pool boiling. The results indicated that the heat transfer coefficients were enhanced slightly. However, critical heat flux increases obviously with greater fin height when the fin thickness remains constant, and with larger fin thickness when the ratio of top fin surface area to projected fin surface area is held constant.

In recent research, micro- or nano-structures were commonly used to enhance pool boiling heat transfer performance. Cooke and Kandlikar [23] studied the effects of microchannel on pool boiling heat transfer performance. Ten different combinations of microchannel width, fin width and channel depth were used in their study. The heat transfer coefficient was enhanced in all cases and the best enhancement was over 5 times

of plain surfaces for the same superheat. Jun et al. [24] developed a nano-textured surface to study pool boiling performance by using ethanol and water as working fluid. The nano-textured surfaces were made of copper covered with copper nanofiber mats. The results indicate that the heat transfer coefficient was enhanced 6 to 8 times in comparison to that bare copper surface. For pool boiling of water, heat transfer coefficient of nano-textured surface was about 3 to 5 times higher than that of bare copper surface. They attributed the enhancement to the fact that the temperature of liquid surrounding the bubble was increased by nano-textured surface and therefore bubble growth was promoted. The effect of the nano-textured surface on the critical heat flux was also investigated in this research. The results showed that the critical heat flux on the nano-textured surface was very close to the bare copper surface cases. However, at the critical heat flux, the superheat on the nano-textured surface was 10 $^{\circ}$C lower than that on the bare copper surface.

2.2.2 Additives for fluid

Fluid properties such as thermal conductivity and surface tension can be changed by using a small amount of additives. Many studies had reported on the effect of the fluids additives on pool boiling heat transfer. Fujita and Bai [25] studied critical heat flux in pool boiling when using seven different binary mixtures in different mole fractions. The results showed that aqueous mixtures of methanol and ethanol improved critical heat flux significantly compared to the interpolated value between pure

components, while the mixtures of methanol/benzene and water/ethylene decreased the critical heat flux by 20% to 50%. They also used a dimensionless Marangoni number to correlate critical heat flux in binary mixtures and the correlation showed a good agreement with the experimental data.

The effects of using nanofluids were first investigated by Choi [26]. A large number of studies have considered the use of nanofluid to improve pool boiling. Bang and Chang [27] studied heat transfer performance of pool boiling of nanofluids which made of alumina nano-particle and water in different volume concentrations. The result showed the nanofluids had worse heat transfer performance than pure water in the nucleate boiling, but the enhancement in critical heat flux were significant in both horizontal and vertical pool boiling. They concluded that the reduction in heat transfer performance could be attributed to the fouling effect caused by the agglomeration of nanoparticles at the surface. This is turn led to poor thermal conductivity and increased roughness caused by high nano-particle concentration at the surface. However, Tu et al. [28] conducted a study on the heat transfer performance of pool boiling using Al_2O_3-H_20 nanofluids and concluded that significant enhancement in both heat transfer coefficient and critical heat flux were obtained. They also observed that there were four times more active nucleation sites and smaller bubble with no obvious change in bubble departure when nanofluids were used. Wen and Ding [29] summarized the conflicting nanofluid pool boiling results, which they attributed to effect of the nanofluids properties, surfactant use, and the interaction between nanofluids and surface. In summary, the agglomeration, sedimentation and contamination in nanofluids were considered to have

an effect on surface properties and the heat transfer coefficient. On the other hand, critical heat flux was enhanced when using nanofluids. Kim et al. [30] investigated the effect of nanofluids (alumina, zirconia and silica particles in water) on the pool boiling critical heat flux. The results showed that the critical heat flux was enhanced at modest nanoparticle concentration. They implied that the improvement of surface wettability caused by the buildup of a porous layer of nanoparticles on the surface resulted in an increased in critical heat flux.

2.2.3 Use of heat transfer enhancers

Heat transfer enhancers have been used for decades to promote better pool boiling in a host of applications. Some enhancers are used to change the motion of the bubbles and fluid near the surface. Nishikawa et al. [31] studied the effects of inclined surfaces on the pool boiling of water. The inclined angle was varied from 0° (upward-facing) to 175° (downward-facing). The results showed that the surface orientation had a significant improvement on heat transfer coefficient at the isolated nucleate boiling regime, but had no influence on heat transfer coefficient at the fully developed nucleate boiling. Two effects have been identified to cause the enhancement of heat transfer. First, according to Hsu's analysis [32], the superheat of nucleate boiling would be lower with increasing thermal boundary layer thickness. Second, on an inclined surface, the sweeping effect that improves vaporization of the liquid film between the bubble and liquid would also enhance the pool boiling heat transfer performance. Katto et al. [33] investigated the pool boiling heat transfer performance in a narrow space by placing a

glass disc above the surface containing vapor bubbles. By changing the gap size, they found out that the heat transfer coefficient could be enhanced while the critical heat flux was decreased with decreasing gap size. With a gap size in the range of 0.2 mm to 2 mm, they attributed the enhancement at lower heat flux to the extremely thin static liquid film between bubble and surface. Rapid evaporation occurs in the thin liquid film which is caused by improvements in heat transfer. However, the heat transfer performance is also affected by gap size. For a small gap size (0.1 mm), the enhancement of the heat transfer coefficient vanishes because of the onset of film boiling. Passos et al. [34] studied pool boiling performance with downward-facing surfaces in a narrow space using horizontal disc with a small gap. The results show that the confined space lead to greater heat transfer coefficient at the lower heat flux but reduced critical heat flux with decreasing the gap size. Rops et al. [35] studied the effects of spatially confined spaces with different pool diameter. The results indicate that heat transfer coefficient increases when pool diameter decreases. They concluded that the improvement of the heat transfer coefficient was caused by stable circulating flow in the smaller confined space; while in the larger confined space, there was no enhancement because only the chaotic and mainly upward motion from boiling could be observed in the fluid. Zhao et al. [36] built and tested a confined space by placing a mesh screen above the surface in the gap. The results showed that the heat transfer coefficient was obviously enhanced in smaller gap size and mesh spacing. The authors concluded that the heat transfer coefficient could be increased when bubbles coalesce and absorb bubbles near the heated surface within the confined space. This also leads to rapid evaporation of the liquid micro-layer between

the coalesced bubble attached to or near the surface, which also disrupts the thermal boundary layer when the bubble grows fast and departs from the surface.

3. EXPERIMENT FACILITIES AND METHODS

This section describes the pool boiling facilities which were designed and built in order to achieve the research objectives and experiment methods which are part of the research project.

3.1 Experiment facilities

The facilities consisted of five parts: the test chamber, the heating element, the data acquisition system, the power supply, and the chiller. The scheme of experimental set up is shown in Figure 3.1 and a photo of it in Figure 3.2. A detailed explanation of all the components of the experimental set up is included below.

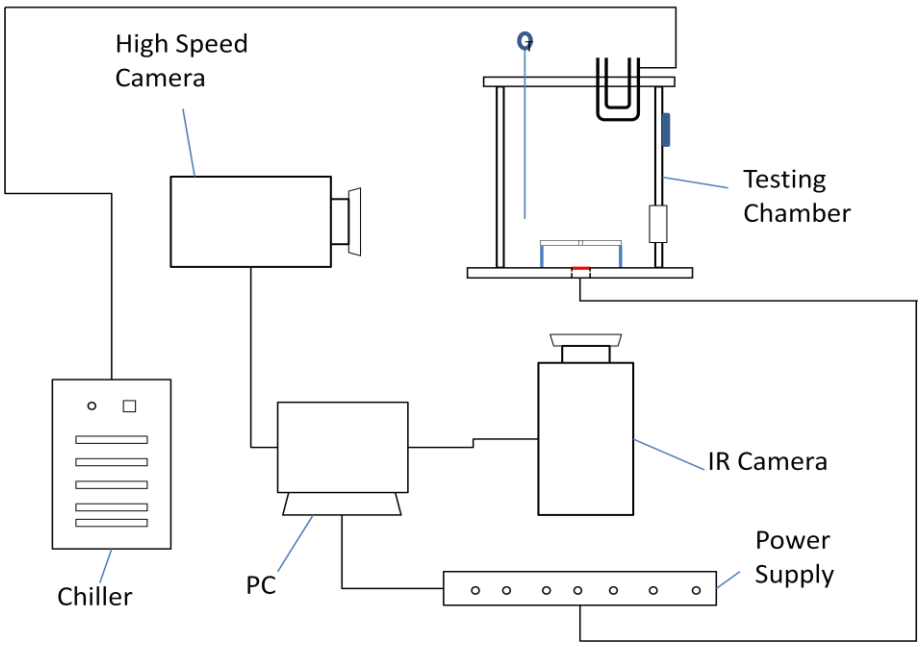

Figure 3.1 Scheme of pool boiling setup

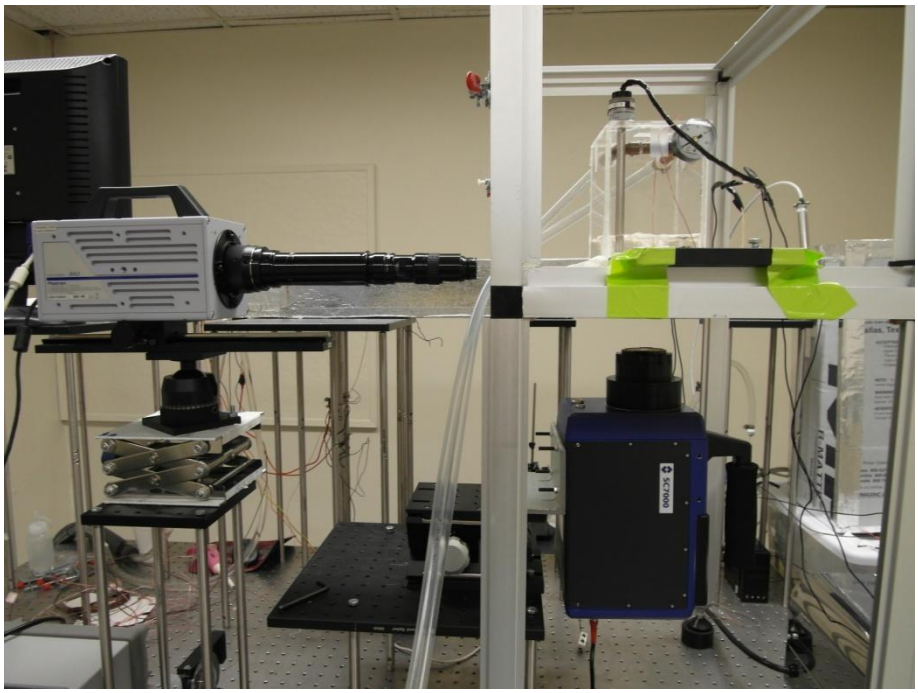

Figure 3.2 Photo of pool boiling setup

3.1.1 Working fluid

Engineered Fluid HFE-7100 (3M^{TM} Novec^{TM}) was used in this research as the working fluid. It was chosen because of its safe handling, good chemical compatibility with most materials, and low boiling temperature (61 ℃). The properties of HFE-7100 are shown in Table 3.1.

Boiling point (℃)	61
Freeze point (℃)	-135
Density (g/ml)	1.52
Vapor density (g/ml)	0.011
Latent heat (J/g)	111.6
Liquid specific heat (J/Kg-℃)	1183
Liquid thermal conductivity (W/m-K)	0.062

Table 3.1 HFE-7100 properties

3.1.2 Test chamber

A test chamber was designed to facilitate the imaging and data collection of confined pool boiling experiments. It consists of a cartridge heater (pre-heater), a temperature switch, a condenser tube, a pressure gauge, and a sample holder as shown in Figure 3.3 and Figure 3.4. The cartridge heater was used to pre-heat the liquid to the saturated temperature before each experiment. It is controlled by a temperature switch which allows the system to remain at the desired temperature. The condenser tube is a U-shape copper tube which is connected to a water-cooled chiller. It was used to condense vapor back to liquid and also ensure constant pressure conditions within the test chamber. The pressure gauge was used to monitor the pressure in the chamber to avoid high pressures.

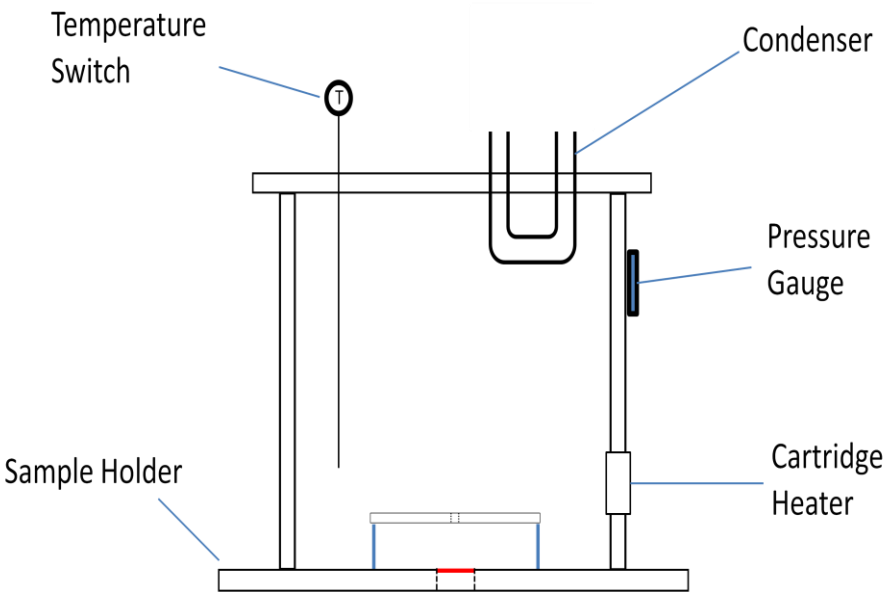

Figure 3.3 Scheme of test chamber

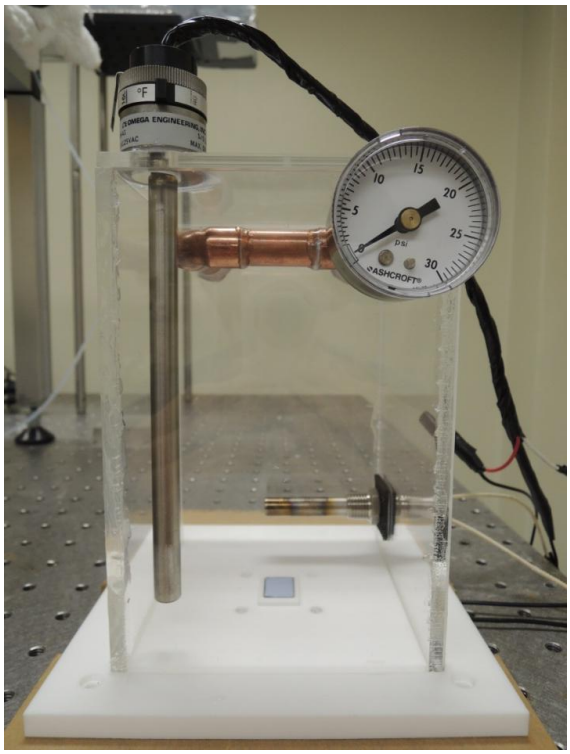

Figure 3.4 Photo of test chamber

A Teflon sample holder was designed to position and secure the heater assembly. The design drawing and 3-D simulation for the holder are shown in Figure 3.5 and Figure 3.6. An adiabatic epoxy (EPO-TEK® OE145, EPOXY TECHNOLOGY) was used to attach the heater to the holder. The holder was also designed to accommodate the hole plate used for the confined pool boiling experiments. Screws were used to secure and position the upper plate which had a hole in the middle position. Washers were used to adjust the gap size of the confined space. In this research, three different hole diameters were used including 2 mm, 3 mm, and 4 mm hole size and three different gap sizes including 2.3 mm (4 washers), 3.6 mm (5 washers), and 5 mm (6 washers). The photo of the confined space is shown in Figure 3.7 and Figure 3.8.

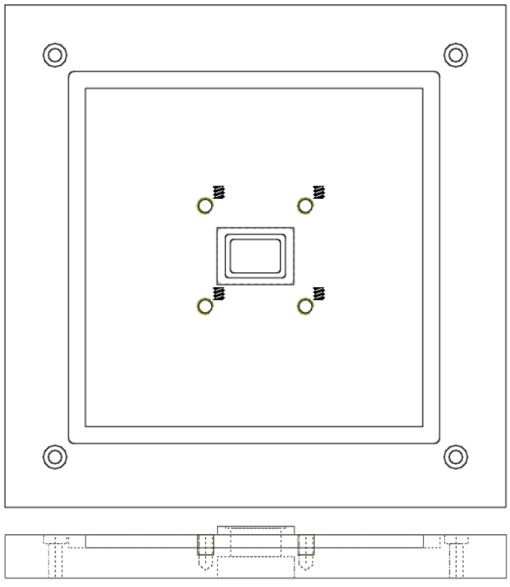

Figure 3.5 Design drawing of sample holder

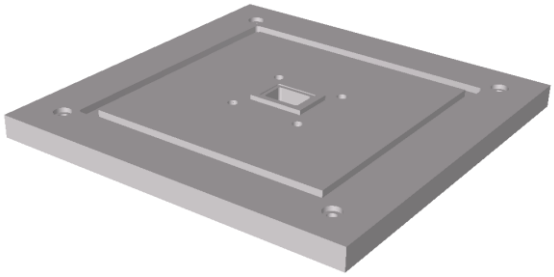

Figure 3.6 3-D simulation of sample holder

Figure 3.7 Top view photo of confined space

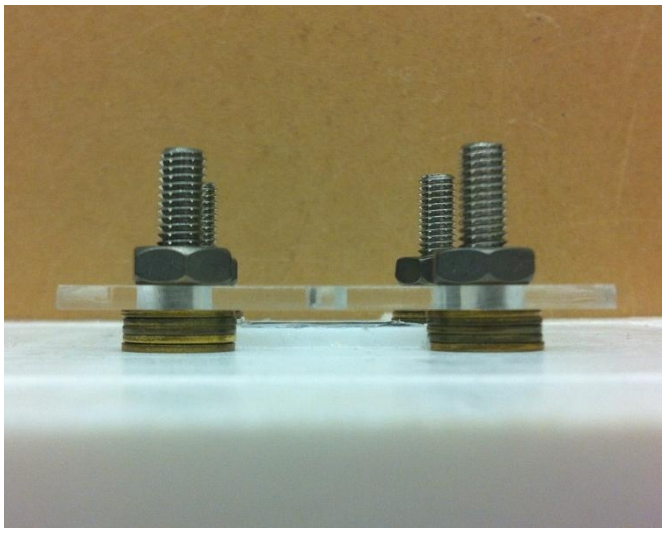

Figure 3.8 Side view photo of confined space

3.1.3 Heating element

In this research, a thin film of Indium-Tin-Oxide (ITO) was deposited on a silicon substrate which was as heating element. The dimensions of the substrate were 17 ×12 mm^2 which were about 17 times and 12 times capillary length of fluid (L_c=0.95 mm), respectively. The ratios of dimensions to the capillary length were large enough to avoid the effect of heater size. Hendricks et al. [37] also designed the heater surface with each side 12 times the capillary length to avoid modulating hydrodynamic instabilities. The wafer thickness was 500 μm, and the thickness of ITO was 100 nm. A small surface area for pool boiling was used in order to avoid the collapse or breakage of the heater surface due to the pressure caused by liquid height inside the pool boiling chamber. Several past studies [22, 39-47] have also considered the use of small heater surfaces in pool boiling studies as described in Appendix B. In the current study, similar surface dimensions

were used where the effects of heater size on bubble nucleation and bubble size are not clearly identifiable. The ITO side was faced downward and attached on the sample holder by using the epoxy mentioned above. Two wires were attached near the edge of ITO coating using the electrically conductive epoxy (MG chemicals epoxy, Allied Electronic) and were connected to a power supply. The scheme of the heating element setup is shown in Figure 3.9.

Silicon wafer was chosen as the substrate of the heater due to its high thermal conductivity which ensured uniform temperature distribution in the axial direction. The properties of silicon wafers are shown in Table 3.2. In this research, ITO coating always faced downward and was never in contact with the working fluid in the test chamber. This was done purposely to simplify the construction of the heater system where the power wires did not have to be immersed in the pool liquid and to avoid the effects of ITO coating roughness on pool boiling phenomena.

Heat loss to the environment also had to be considered when using the heater element set up. Detailed estimations of the heat loss analysis are shown in the following section.

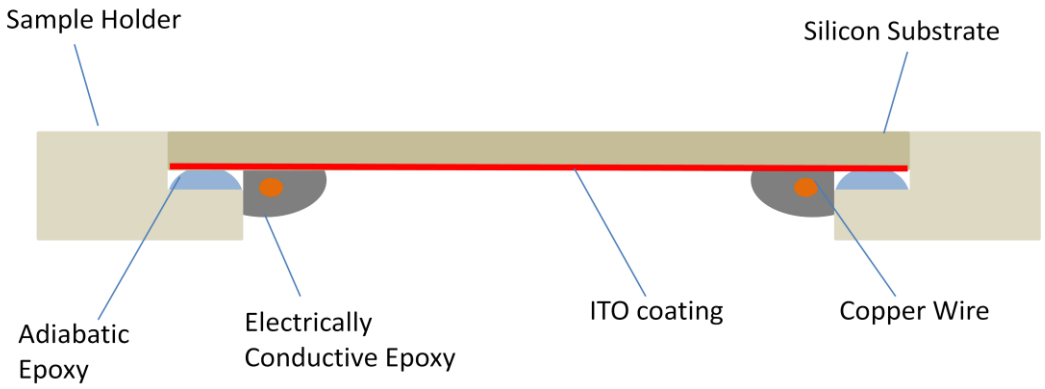

Figure 3.9 Scheme of heating element setup

Density (g/ml)	2.33
Melting point (℃)	1414
Specific heat (J/g-℃)	0.7
Thermal conductivity (W/m-K)	148
Thermal diffusivity (cm^2/s)	0.8

Table 3.2 Properties of silicon wafer

3.1.4 Data acquisition system

3.1.4.1 Infrared camera

The temperature distributions on the heater surface were acquired by using an infrared camera (SC7650-MB, FLIR system, Inc) with 50 mm MW lens (L0106) which was located below the heater. Two extension rings, 12 mm and 20 mm, were also used with the 50 mm lens. The photo of IR camera is shown in Figure 3.10. The full resolution of infrared camera was 640×512 pixels, but the effective area was only a

circular area with approximately 240 pixels diameter. The infrared camera has a spatial resolution of about 25 µm per pixel and the frame capture rate was set to 100 Hz at the full frame. In this research, 100 Hz frame capture rates with a 640x512 pixel resolution was used. With the FLIR Indigo InSb type sensor, the IR wavelength range of the infrared camera was between 1.5 and 5.1 µm (near IR to middle IR). The software, ExaminIR was used to record the temperature distribution video by importing variables such as emissivity, reflective temperature, frame rate, and the working temperature. The average surface temperature was obtained by calculating the spatial average temperature for each IR image, then calculating the temporal average temperature for the IR images in one second. The spatial and temporal standard deviations of surface temperature were also obtained in order to check the accuracy of the surface temperature measurement as described in Section 4.1.

Figure 3.10 Infrared camera SC7650-MB with lens

3.1.4.2 High speed camera

A high speed camera (FASTCAM SA3, Photron) with a high resolution lens (Zoom 6000 series, Navitar) was used to capture the high speed video of the bubble motion. A photo of the camera is shown in Figure 3.11. The maximum resolution of the high speed camera was set to 1024×1024 pixels when the frame rate was set at 1000 Hz. High speed images were recorded by FASTCAM viewer by setting the desired resolution, frame rate, shutter speed and trigger mode.

Figure 3.11 High speed camera FASTCAM SA3 with lens

3.1.5 Power supply

The power supply used in this research was a Programmable DC Power Supply (GEN600-2.6, Lambda TDK). The maximum voltage was 600V and the maximum current was set at 2.6A for this power supply. It was controlled via a PC using Hyperterminal version 5.1.

3.1.6 Chiller

A chiller (NESLAB Merlin M25, Thermo Scientific) was connected to the condenser tube to control the temperature of condenser. The temperature range of the chiller was set between -15 ℃ and 35 ℃. In this research, the temperature was set at 20 ℃.

3.2 Experimental method

This section describes the experimental procedure and the methods used in this research including emissivity measurement, heat loss estimation and uncertainty analysis.

3.2.1 Emissivity measurement

In this research, the standard ASTM E1933 "Standard test methods for measuring and compensating for emissivity using infrared imaging radiometers" was used to measure the emissivity of the heater surface. In this method, the emissivity of the object was acquired by using a material of known emissivity as reference. Equation 3.1 was then used to calculate the emissivity of the sample.

$$\varepsilon_{tgt} = \frac{D_{tgt} - D_{bkg}}{D_{ref} - D_{bkg}} \varepsilon_{ref} \tag{3.1}$$

Where D is the digital value of the camera in number of counts, and the subscript *tgt* is the target, *ref* is the reference and *bkg* is the background.

The first step consists of measuring the digital value of irradiance from the background where the sample is located. This is done by placing a reflective foil on the ceramic pad and recording the digital counts that emanate from the reflective foil. The reflective foil only allows background IR radiation to reach the IR camera.

Next, the material with known emissivity (vinyl electrical tape 88, ε_{ref} = 0.95±0.05) was attached on the ceramic pad next to the heater. The ceramic pad with the reflective tape and the heater were heated by using the laboratory oven to about 60 ℃, which was at least 30 ℃ higher than room temperature.

Finally, the ceramic pad with the tape and the heater were taken out from the oven quickly and the digital counts of the tape (D_{ref}) and the heater (D_{tgt}) were measured by using the infrared camera. The emissivity of heater was calculated by using equation 3.1.

The process of temperature measurement was repeated by heating the ceramic pad with the tape and the heater at different temperatures. The calculated emissivity values at different temperatures are shown in Figure 3.12.

The emissivity of the sample was 0.4±0.022. The uncertainty of the measurement is about 5.5%. A detailed analysis of emissivity uncertainty can be found in the appendix.

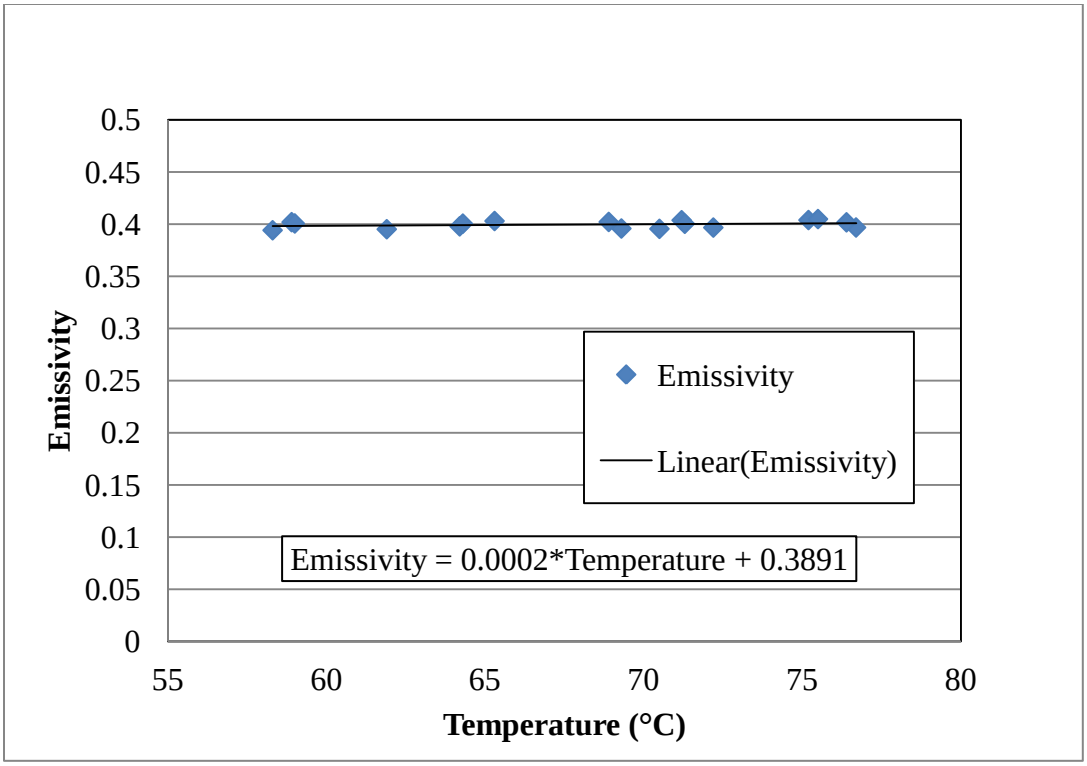

Figure 3.12 Emissivity value of heater at different temperatures

3.2.2 Heat loss estimation

The factors causing heat loss when using the described set up included convection through air and conduction through the sample holder and the electrodes. In order to estimate the total heat loss, experiments were undertaken without working fluid in the test chamber. The surface was heated using small power by controlling the power supply. Then, the surface temperature was recorded once the system reached the steady state condition. Heat loss was determined by knowing the temperature difference between the heater and the surrounding. The relation between power input (heat loss)

and temperature difference between the heater and the surrounding is shown in Figure 3.13.

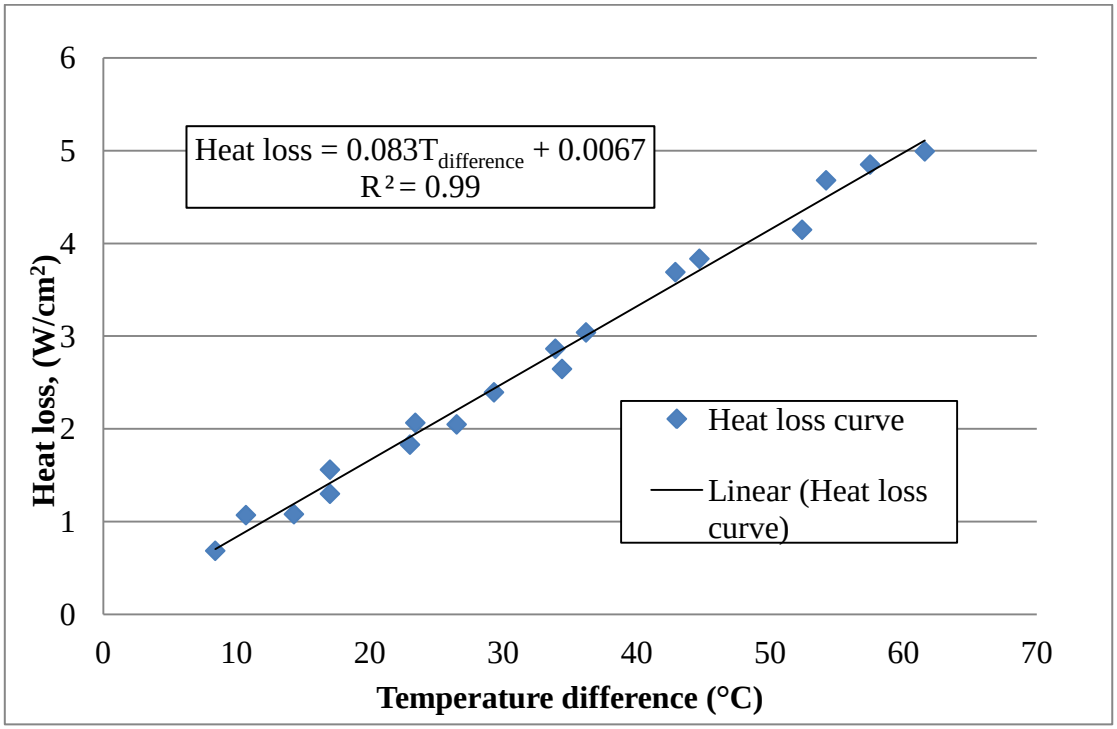

Figure 3.13 Calibration of heat loss corresponding to different temperature difference

3.2.3 Procedure

Before conducting the heat transfer experiment, the heater surface was cleaned using methanol. The chamber was then filled with HFE-7100 liquid until approximately 50 mm liquid level was reached. Then, the system was sealed carefully.

In this research, all the experiments were operated at atmospheric pressure and saturated temperature of HFE-7100. Prior to running the experiments, the working fluid was heated to its saturated temperature using the pre-heater for about 30 minutes in order

to degas the working fluid and allow the system reach the saturated temperature of HFE-7100. The heater was then powered by adjusting the power supply voltage. Power delivered from the power supply was calculated by taking into account current and voltage as well as the estimated heat losses. In order to avoid any damage to the heater system, the system was never allowed to reach critical high heat flux values and the voltage was increased in small steps. The heat flux from the surface into the liquid also was calculated as follows:

$$q'' = \frac{Q_{in} - Q_{loss}}{A} \tag{3.2}$$

During each experiment, high speed images were captured by using the high speed camera. Based on the procedure used in the previous research [38], the data of surface temperature was acquired in the steady-state experiments when the surface temperature was constant. The temperature field of the surface was recorded by using infrared camera once the heater reached steady-state. The temporal standard deviation of surface temperature can be used to examine whether the temperature of heater surface was constant.

3.2.4 Uncertainty analysis

The method which was used for uncertainty analysis in this research is based on the Kline-McClintock methodology.

Where R is the function with n independent variables, v_1, v_2,……, v_n, as follows:

$$R = R(v_1, v_2, \dots\dots, v_n) \tag{3.3}$$

The equation of uncertainty of R is as follows

$$w_R = \left[\left(\frac{\partial R}{\partial v_1} w_1\right)^2 + \left(\frac{\partial R}{\partial v_2} w_2\right)^2 + \cdots + \left(\frac{\partial R}{\partial v_n} w_n\right)^2\right]^{1/2} \tag{3.4}$$

where w means the uncertainty interval.

More detailed uncertainty analyses of equipment and measurement can be found in the appendix A.

4. RESULTS AND DISCUSSION

In this section, heat transfer performance of confined space pool boiling is presented based on experimental observations. First, the acquirement of baseline in unconfined pool boiling is presented. Second, results of pool boiling when using a plate with different gap sizes are presented. Then, the effects of plate hole diameter on heat transfer are also discussed. Bubble images in the confined space are shown in order to explain how their movement has an effect on heat transfer enhancement. Calculation and analysis of bubble frequency and bubble diameter have been obtained based on bubble images and used to explain heat transfer performance. Finally, comparison between confined pool boiling cases when single hole and triple hole plates were used are shown and discussed.

4.1 Unconfined pool boiling

In this research, the boiling curve of unconfined pool boiling was obtained is used as the baseline compared with the curve of confined pool boiling. In order to obtain the boiling curve, the average surface temperature and heat flux were measured simultaneously. As discussed in section 3.1.4.1, the average surface temperature values were acquired by calculating the spatial and temporal average temperature from the IR images as shown in Figure 4.1. Heat flux values were calculated using Equation 3.2 as discussed in the section 3.2.3. The spatial standard deviation of the surface temperature ranged between 0.4 ℃ and 0.6 ℃ for each IR images whose size is 4 mm by 4 mm (or less than 8% of the total heater area). This indicates the unconfined pool boiling process

was rather homogenous due to the formation, growth and detachment of hundreds of small bubbles. The temporal standard deviation ranged from 0.02 ℃ and 0.04 ℃ which was based on 100 consecutive IR images corresponding to one second of uniform heat flux applied to the surface. The small temporal standard deviation can be attributed to the relatively fast bubble nucleation, growth and detachment processes, which typically take place in 10 ms or in one IR snapshot image. Therefore, the IR system only captures time-averaged (fast) processes resulting in rather constant surface temperature values. On the other hand, boiling in confined spaces is characterized by spatial standard deviation of surface temperature ranging between 0.4 ℃ and 0.8 ℃ within each IR image, while the temporal standard deviation ranged between 0.1 ℃ and 0.3 ℃ for 100 consecutive IR images in one second. The greater spatial standard deviation in the confined space when compared to the unconfined pool boiling case can be attributed to the formation of large coalesced bubbles which induce shear flow within the confined space. The shear flow in turn affects the surface temperature distribution as the values of the spatial standard deviation suggest. This is discussed in greater detail below. Boiling curve for unconfined pool boiling is shown in Figure 4.2 and the bubble images captured by high speed camera are shown in Figure 4.3. The errors of heat flux and superheat values in the repeated experiments were also computed as shown in Figure 4.2. The uncertainty in the heat flux value is less than 2% as shown in Appendix A, and the standard deviation of the measurement of temperature was less than 0.6 ℃ (less than 2% in error) for each point. The small errors indicate that the experiments are entirely reproducible. Furthermore, the average temperature rate during the experiments never

exceeded of 0.005 ℃/sec. The ΔT (T_w - T_{sat}) for onset of nucleate boiling (ONB) in the unconfined case correlates well with past studies conducted using similar dielectric fluids as shown in the Appendix B.

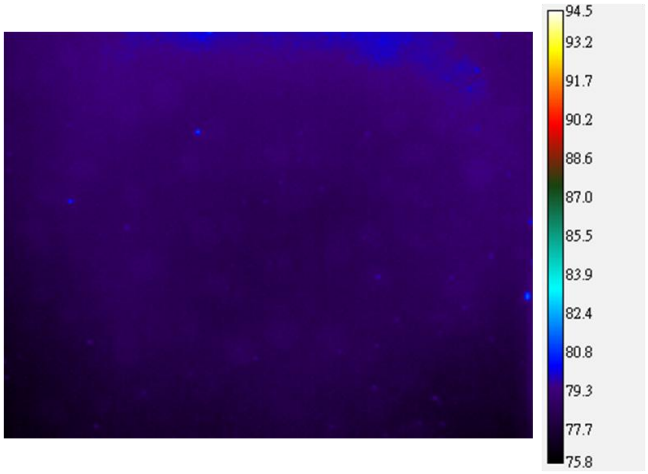

Figure 4.1 Surface temperature map acquired using IR camera in unconfined pool boiling at 18 W/cm^2

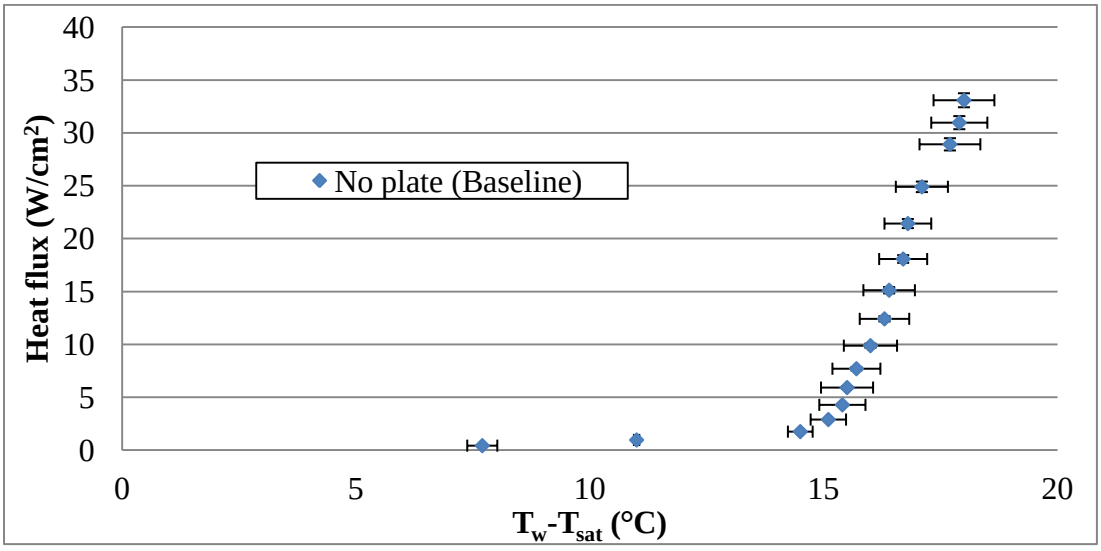

Figure 4.2 Boiling curve of unconfined pool boiling

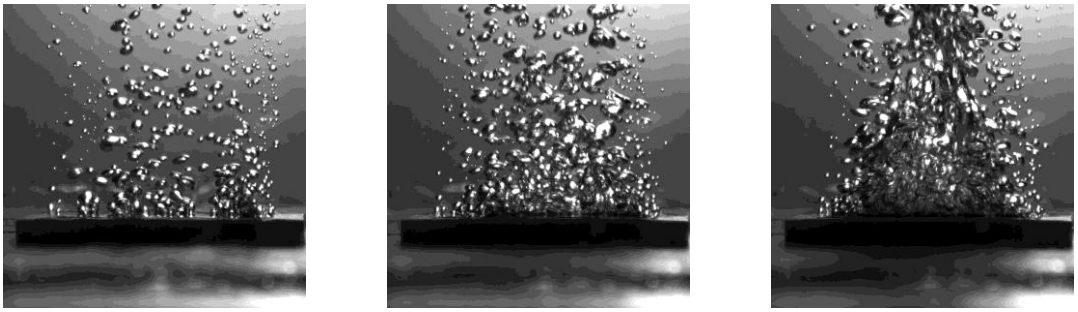

(a) (b) (c)

Figure 4.3 Bubble images of unconfined pool boiling at (a) 6 W/cm^2 (b) 15 W/cm^2 (c) 33 W/cm^2

4.2 Effect of plate gap size on confined pool boiling phenomena

The effects of plate gap size on confined pool boiling phenomena were identified and quantified by comparing the boiling curve of confined pool boiling to the baseline shown in Figure 4.2. Figures 4.4 to 4.6 show the boiling curve when different gap sizes were used with a single hole plate. The hole diameters were 2 mm, 3 mm, and 4 mm. The standard deviation values of surface temperature value in repeated experiments were less than 0.7 ℃ (less than 3% error) in all cases. Error bars for standard deviation in Figures 4.4 to 4.6 can be found in the Appendix C. The cases A to I shown in Table 4.1 are represented to the cases in the different combination of gap size and hole diameter.

		Gap Size (mm)		
		2.3 mm	3.6 mm	5 mm
Hole	2 mm	Case A	Case B	Case C
	3 mm	Case D	Case E	Case F
	4 mm	Case G	Case H	Case I

Table 4.1 Cases table

For the cases of the 2 mm hole diameter (cases A – C) shown in Figure 4.4, the optimum heat transfer performance was achieved when the lowest gap (2.3 mm, case A) at low heat flux (less than 10 W/cm^2) was used. The boiling curve for case A depicts a maximum reduction of surface temperature of about 4 ℃ at the onset of nucleate boiling (ONB). However, in the moderate heat flux region (10 - 20 W/cm^2), the surface temperature in this case is higher than that in the no plate case because the "dryout" conditions appears at lower surface temperature. The dryout results from the bubble flow restriction caused by the 2 mm hole itself. For the 3.6 mm gap (case B), slight enhancement is observed from Figure 4.4. The boiling curve in case (B) is characterized by a slight reduction in surface temperature of about 0.4 ℃ to 0.6 ℃. On the other hand, the boiling curve for the 5 mm gap case (case C) is the closest to the baseline case, which indicates no improvement in heat transfer in the case C.

For the cases of 3 mm hole diameter (case D – F), when the heat flux value is less than 15 W/cm^2, heat transfer performance is improved in case D and E, and especially enhanced at ONB for case D as shown in Figure 4.5. The maximum decrease

in surface temperature in the case D is 2.1 ℃ at ONB, while the reduction in surface temperature for the case E is about 0.5 ℃ to 0.9 ℃ in the same heat flux region. The dryout phenomenon is also observed in these cases when the heat flux value is about 18 W/cm^2. On the other hand, in the case F, no significant enhancement is observed.

In the case of 4 mm hole diameter (case G – I), heat transfer performance is enhanced optimum when a 2.3 mm gap (case G) is used as shown in Figure 4.6. Furthermore, the surface temperature is about 1 ℃ less when compared to the baseline. However, for the cases when the gap sizes are 3.6 mm and 5 mm (case H and I), the boiling curves are similar to the baseline.

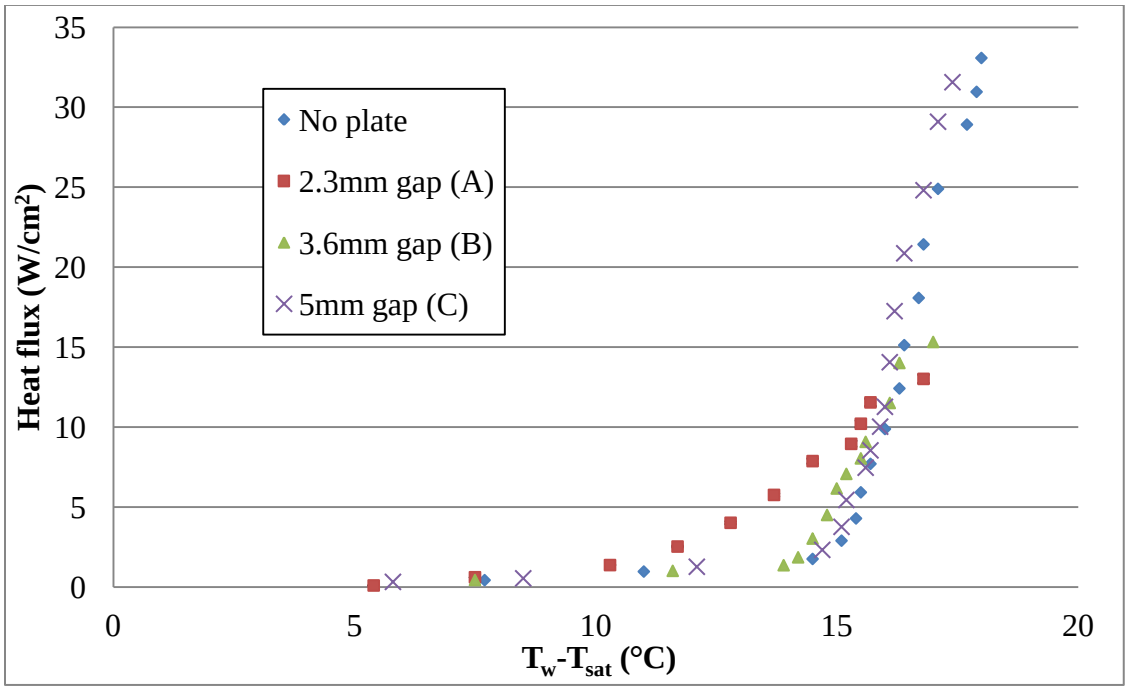

Figure 4.4 Boiling curve of confined space with 2 mm hole plate, Case A – C

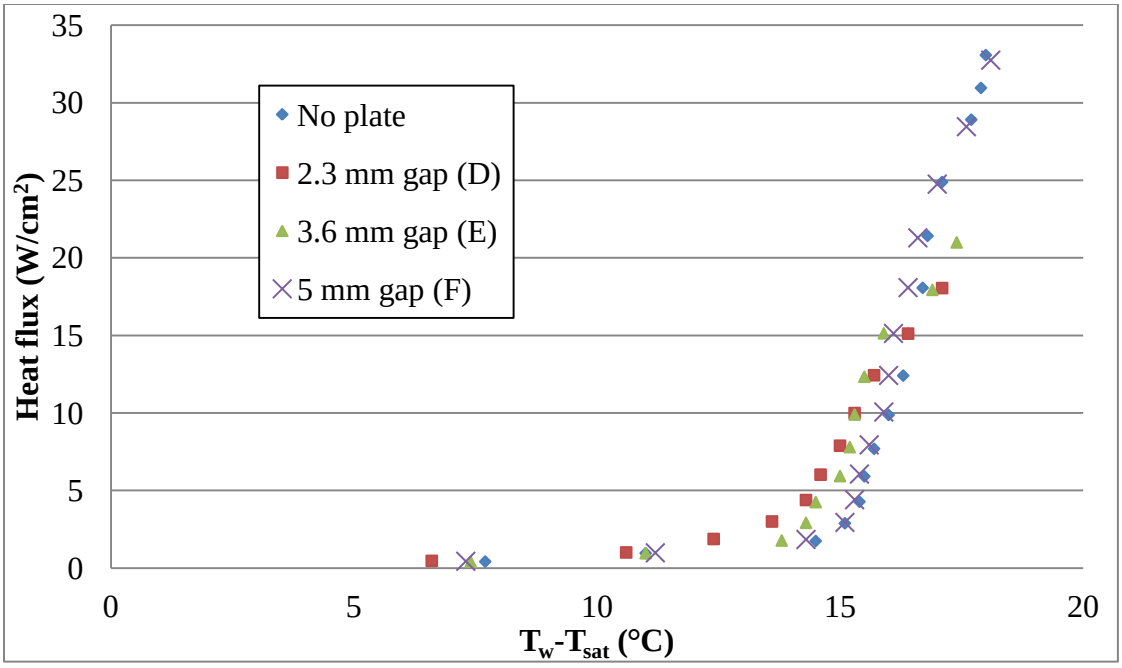

Figure 4.5 Boiling curve of confined space with 3 mm hole plate, Case D – F

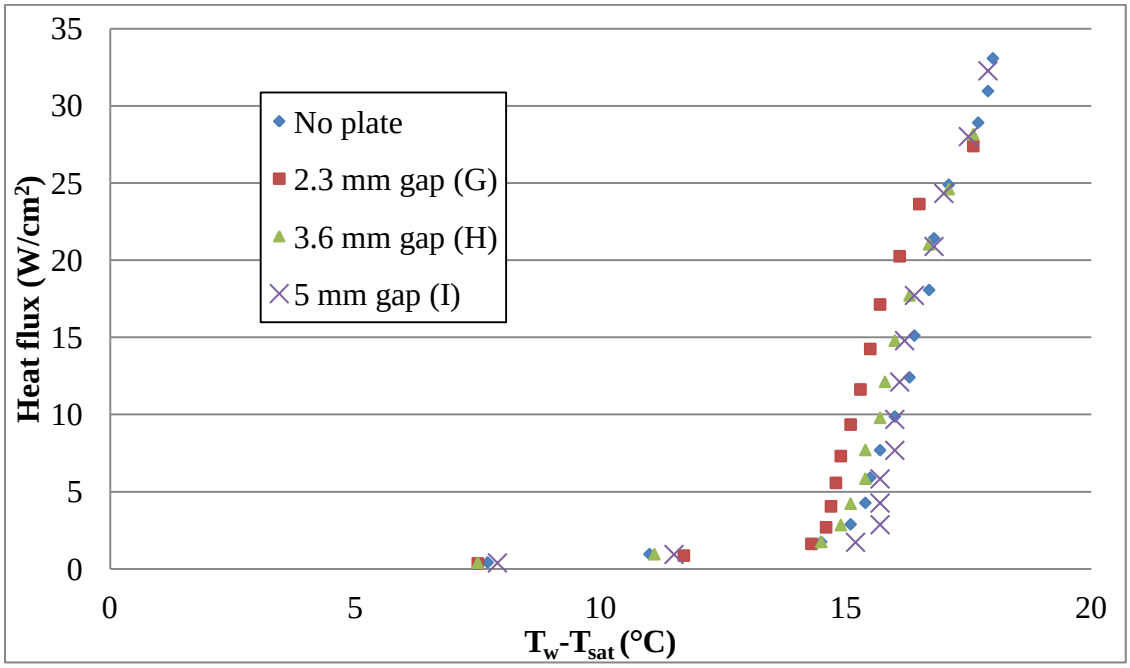

Figure 4.6 Boiling curve of confined space with 3 mm hole plate, Case G – I

Table 4.2 summarizes all results when different gap sizes and hole diameters were used. From Table 4.2, the effect of gap size is noticeable. The confined space with a 2.3 mm gap performs better than the 3.6 mm and 5 mm gap cases from the heat transfer point of view. On the other hand, there is no enhancement in heat transfer performance when the gap size is 5 mm in all the three diameter cases. The difference in heat transfer performance when different gap sizes are used can be attributed to the bubble and fluid motion within the confined space. Figures 4.7 to 4.9 show the side and top views of bubbles when the hole diameter was set to 2 mm, 3mm, and 4 mm. These images can be used to explain the bubble and fluid motion in the confined spaces.

		Gap Size (mm)		
		2.3 mm	3.6 mm	5 mm
Hole Diameter (mm)	2 mm	• Enhanced in the low heat flux region • Temperature reduction: 1.1 ℃ – 4 ℃	• Slightly enhanced in the low heat flux region • Temperature reduction: 0.4 ℃ – 0.6 ℃	• No enhancement
	3 mm	• Enhanced in the low heat flux region • Temperature reduction: 0.8 ℃ – 2.1 ℃	• Slightly enhanced in the low heat flux region • Temperature reduction: 0.5 ℃ – 0.9 ℃	• No enhancement
	4 mm	• Enhanced in all heat flux regions • Temperature reduction: about 1℃	• No enhancement	• No enhancement

Table 4.2 Effects of gap and hole size on confined pool boiling performance

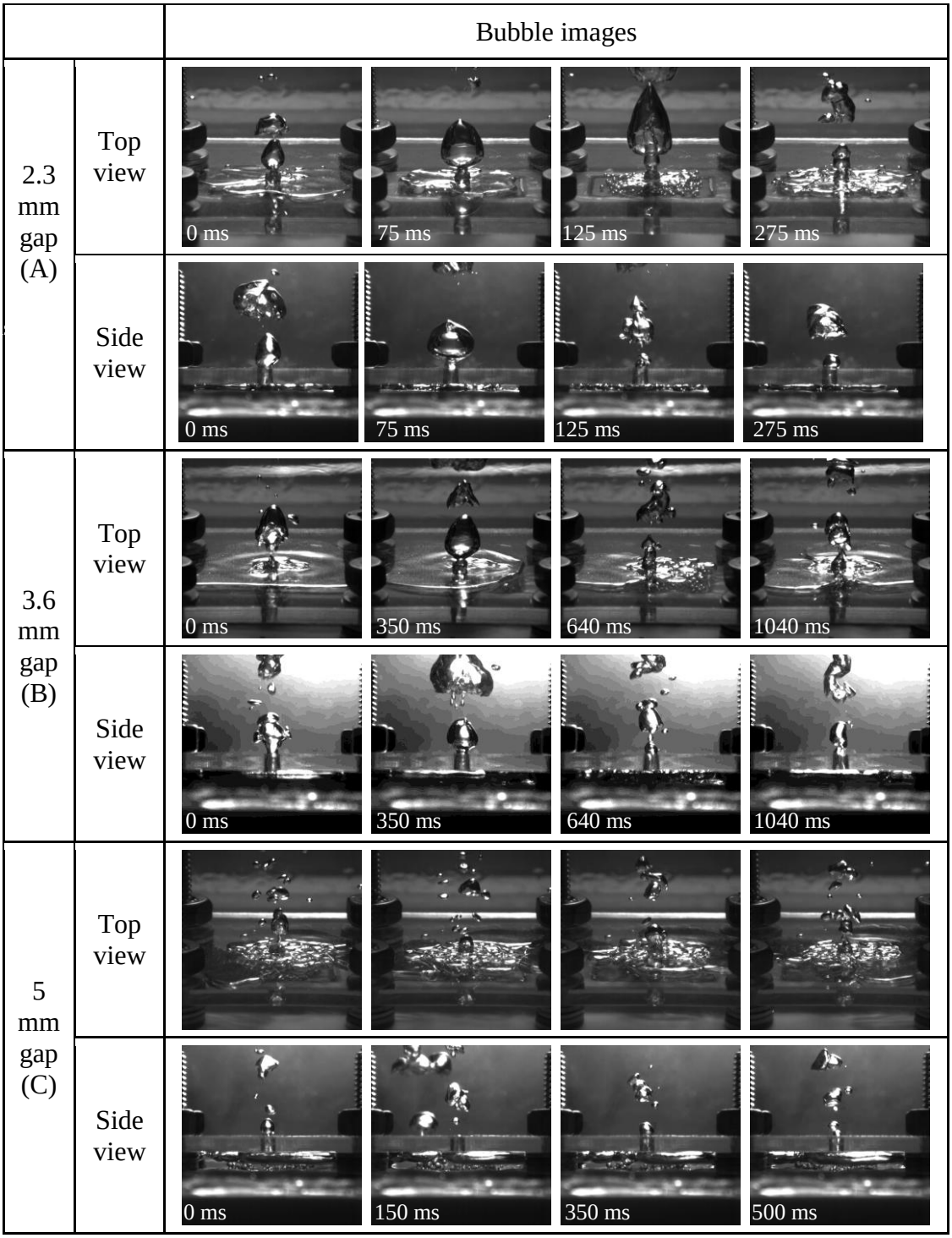

Figure 4.7 Bubble images in confined space with 2 mm hole plate, 5.75W/cm^2

		Bubble images
2.3 mm gap (D)	Top view	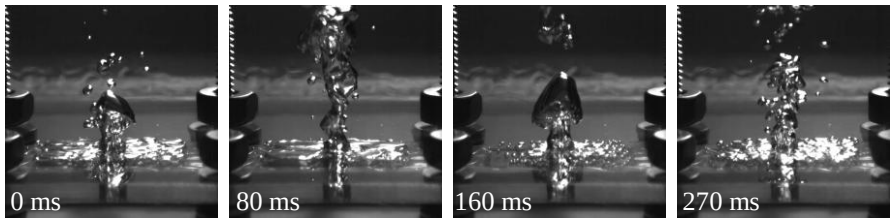
	Side view	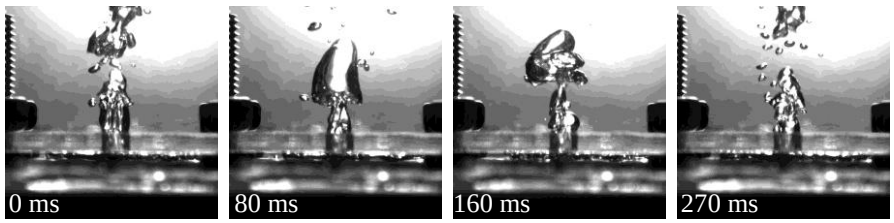
3.6 mm gap (E)	Top view	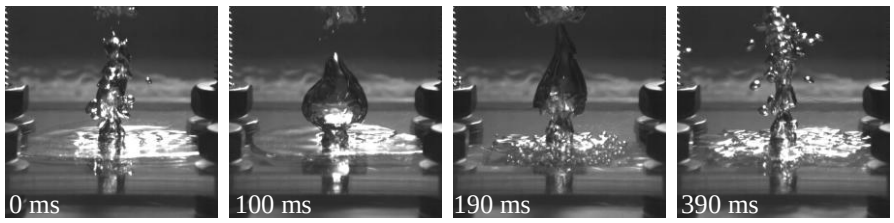
	Side view	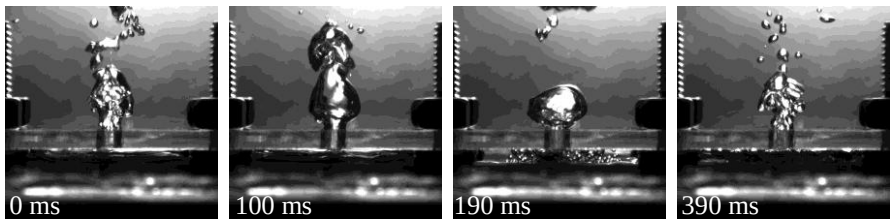
5 mm gap (F)	Top view	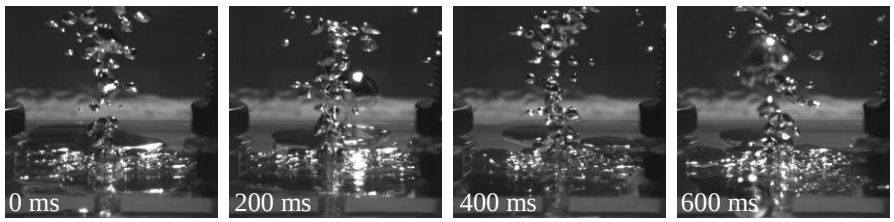
	Side view	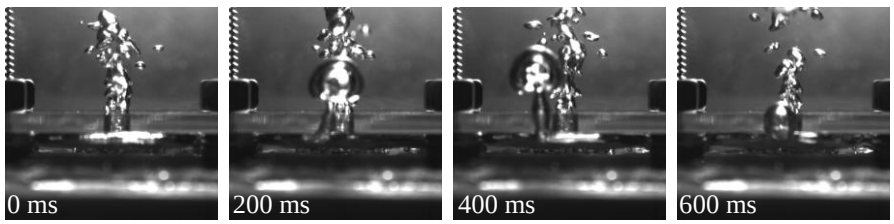

Figure 4.8 Bubble images in confined space with 3 mm hole plate, 8W/cm^2

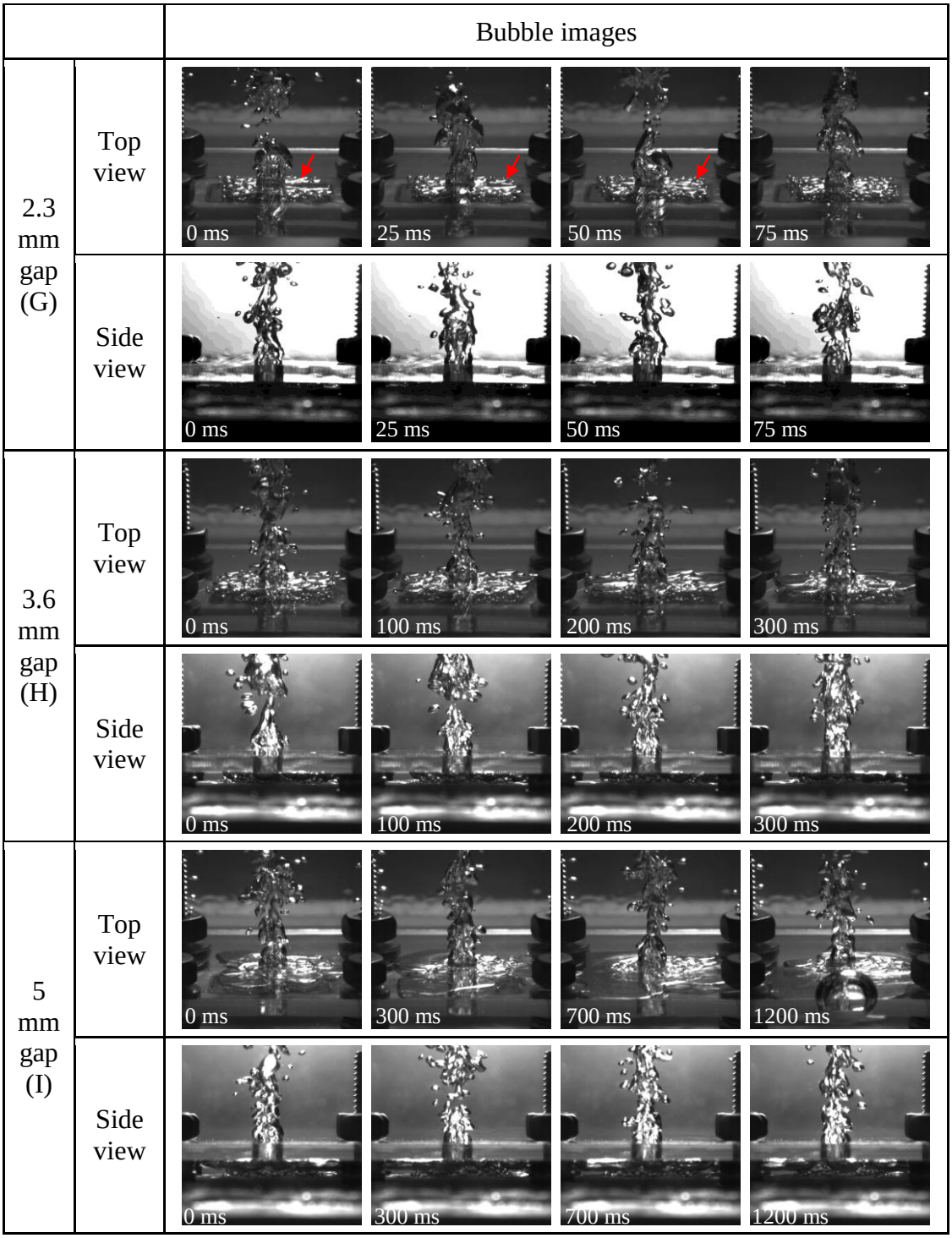

Figure 4.9 Bubble images in confined space with 4 mm hole plate, 9.5W/cm^2

From Figures 4.7 to 4.9, the better heat transfer performance is seen when the gap is fixed at 2.3 mm (case A, D and G). The enhanced performance can be attributed to the induced shear flow caused by the departure of the coalesced bubble through the orifice hole. From the top view images of case A and D shown in Figure 4.7 and 4.8, it is observed that the coalesced bubble departs through the hole followed by the growth of the coalesced bubble inside the confined space. When the coalesced bubble departs through the hole, outside liquid is drawn into the confined space again as intermittent shear flow. The effect of shear flow can be observed in the IR images shown in Figure 4.10. The presence of an intermittent shear flow induced by bubble departure is evident because of the sudden decrease in surface temperature as seen in Figure 4.11. For the case G, although the behavior of coalesced bubble cannot be observed clearly, the induced shear flow can still be detected since small bubbles can be drawn into the holes, which has a direct effect on heat transfer performance. Figure 4.9 shows a small vapor bubble indicated by the arrow which shows how it moves through the hole in a very short time. A similar behavior has been reported by Zhao et al. [36] and Rops et al. [35]. Both publications indicate that fluid motion leads to the improvement in pool boiling heat transfer.

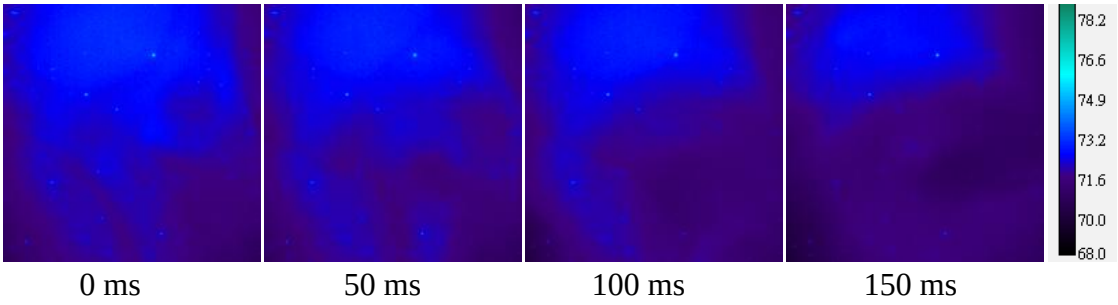

Figure 4.10 IR images in the confined space when the coalesced bubble departs through the hole

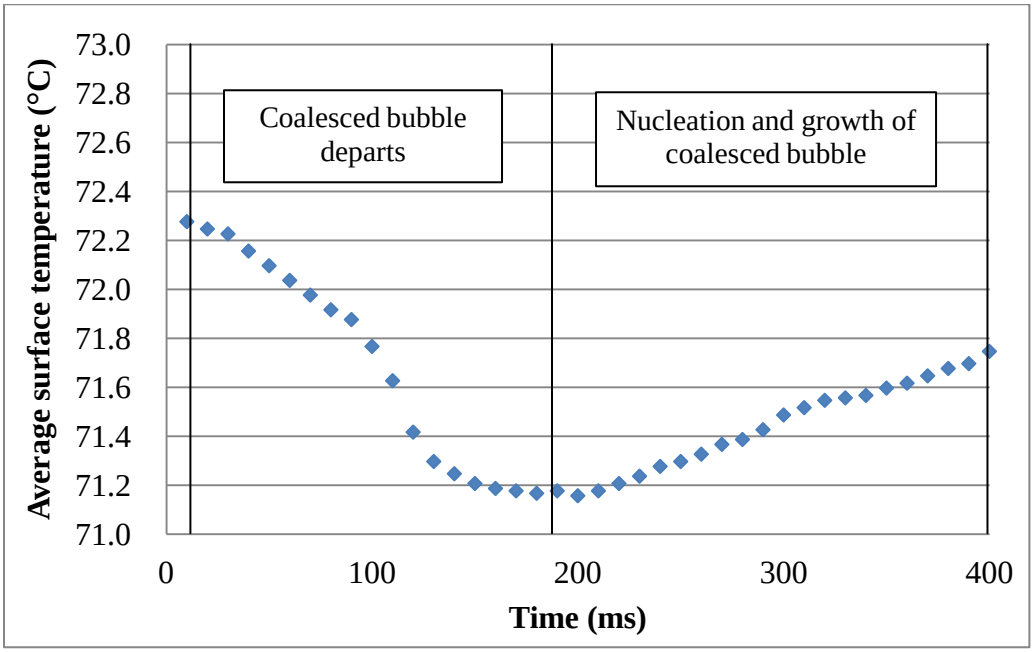

Figure 4.11 Temporal surface temperature in the confined space when the coalesced bubble forms and departs

However, the influence of shear flow in heat transfer performance decreases when the gap size is 3.6 mm or greater. In the cases B and E, departure and growth of coalesced bubbles still can be observed from Figures 4.7 and 4.8, but the coalesced bubble takes more time to depart and grow due to larger confined space available which

reduces the magnitude of the shear flow. These factors lead to small enhancement in heat transfer performance. For the case C and F, the coalesced bubbles are pushed out by the rising smaller bubbles as seen in the top view in Figures 4.7 and 4.8. From the side view in Figures 4.7 and 4.8, it can be also observed that the liquid layer between coalesced bubble and heater surface is significant, which suggest that confined space is too large to have a significant effect on fluid and bubble motion near the surface. Furthermore, the heat transfer performance is similar to the case when there is no plate on top of the heated surface.

On the other hand, in the case H, bubbles are accumulated in the confined space and only few small bubbles forming near the hole can depart easily until the coalesced bubble departs. For case I, the motion of the coalesced bubble is similar as for the case C and F. Furthermore, the boiling curve of all confined cases when the gap was set to 5 mm was found to be similar to the unconfined pool boiling case.

4.3 Effect of plate hole diameter on confined pool boiling

From the result summarized in Table 4.2, the confined space with the 2.3 mm gap depicts the best heat transfer performance when three different hole diameters were used. In this section, all the 2.3 mm gap cases are compared and analyzed to study the effect of hole diameters on the confined pool boiling heat transfer performance. Figure 4.12 shows the boiling curve for three different hole diameters. As it can be seen, case A depicts the best heat transfer performance at the heat flux value less than 8 W/cm^2.

The enhancement percentage of the heat transfer coefficient were calculated using equations 4.1 and 4.2. The uncertainty of the calculation of percentage in heat transfer enhancement is about 5% in the all points.

$$h = \frac{q''}{\Delta T} \tag{4.1}$$

$$\text{enhancement } \% = \frac{(h_{confined} - h_{unconfined})}{h_{unconfined}} \times 100\% \tag{4.2}$$

Figures 4.13 and 4.14 show the enhancement percentages of heat transfer coefficients as a function of heat flux and superheat (ΔT), respectively. Figure 4.13 clearly shows that most of the enhancement takes place in the low heat flux region near ONB. It can be also observed that the confined space in a 2.3 mm gap with the larger hole has the better performance in the higher heat flux region.

As seen in Figure 4.14, heat transfer coefficient enhancement is very significant when compared to the unconfined pool boiling case at superheat values in the range of 12 to 15 ℃. Furthermore, the smallest hole size shows the greatest level of enhancement when compared to the other hole sizes when ΔT is between 14 and 15 ℃. This behavior suggests that there is an optimum surface temperature which results in the formation and departure of a large number of small bubbles from the surface that can effectively be absorbed or driven by the large coalesced bubble as it flows through the orifice. This also suggests that the formation of small bubbles at the surface should be synchronized with the rate of coalesced bubble departure to be able to enhance heat transfer performance.

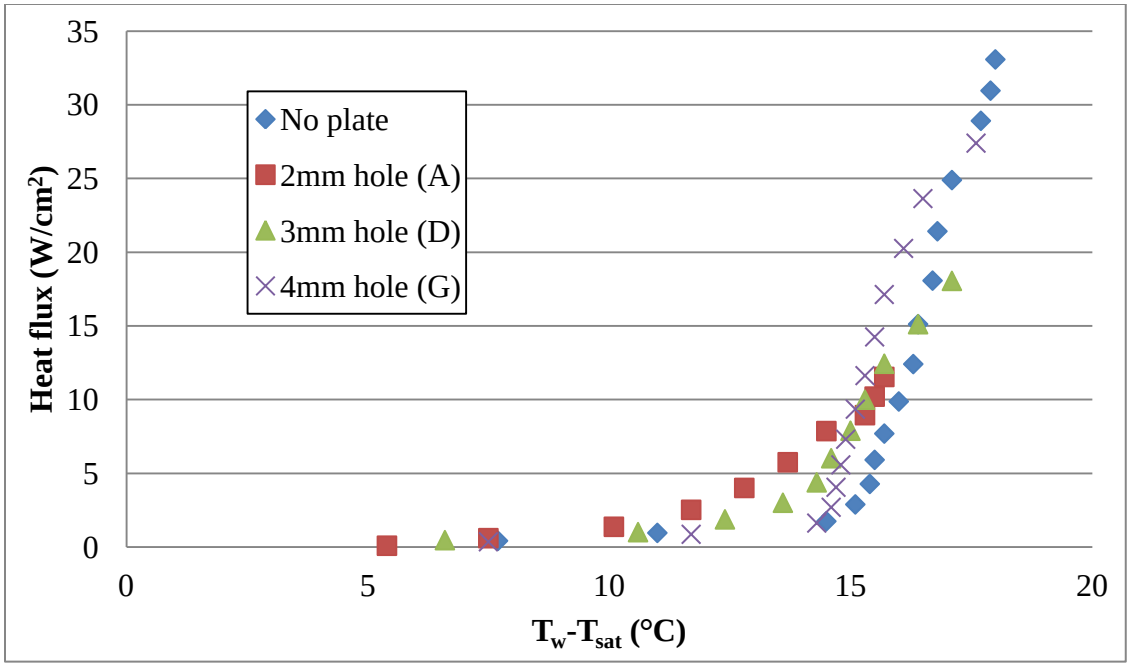

Figure 4.12 Boiling curve of confined space in 2.3 mm gap, case A, D and G

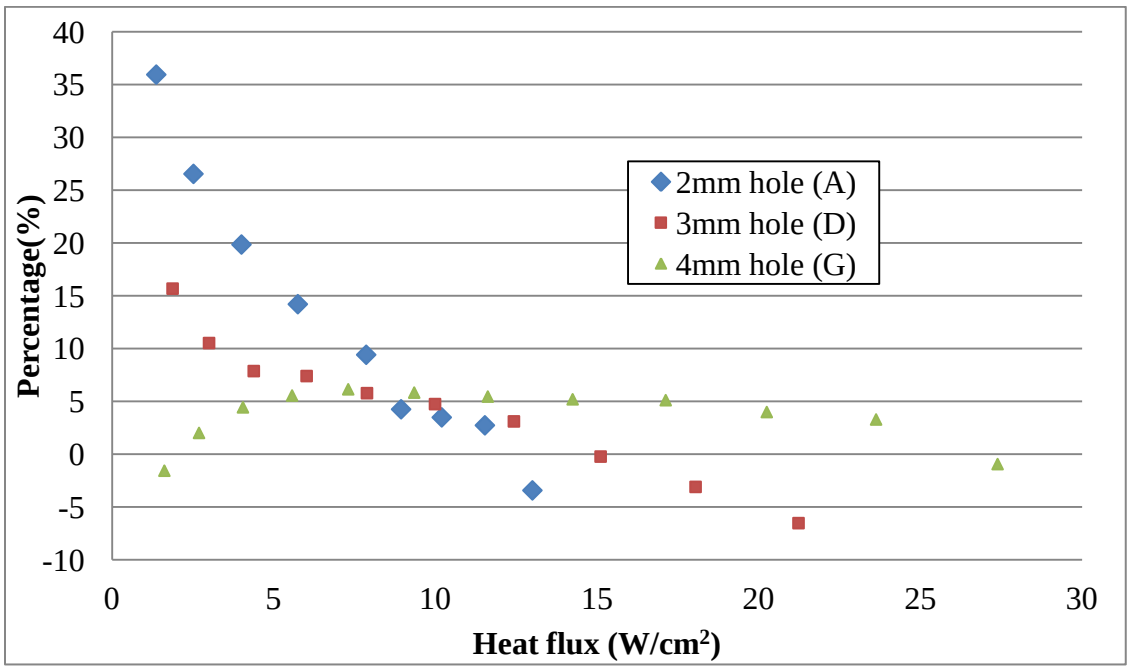

Figure 4.13 Percentage of enhancement in heat transfer coefficient as a function of heat flux, case A, D, and G

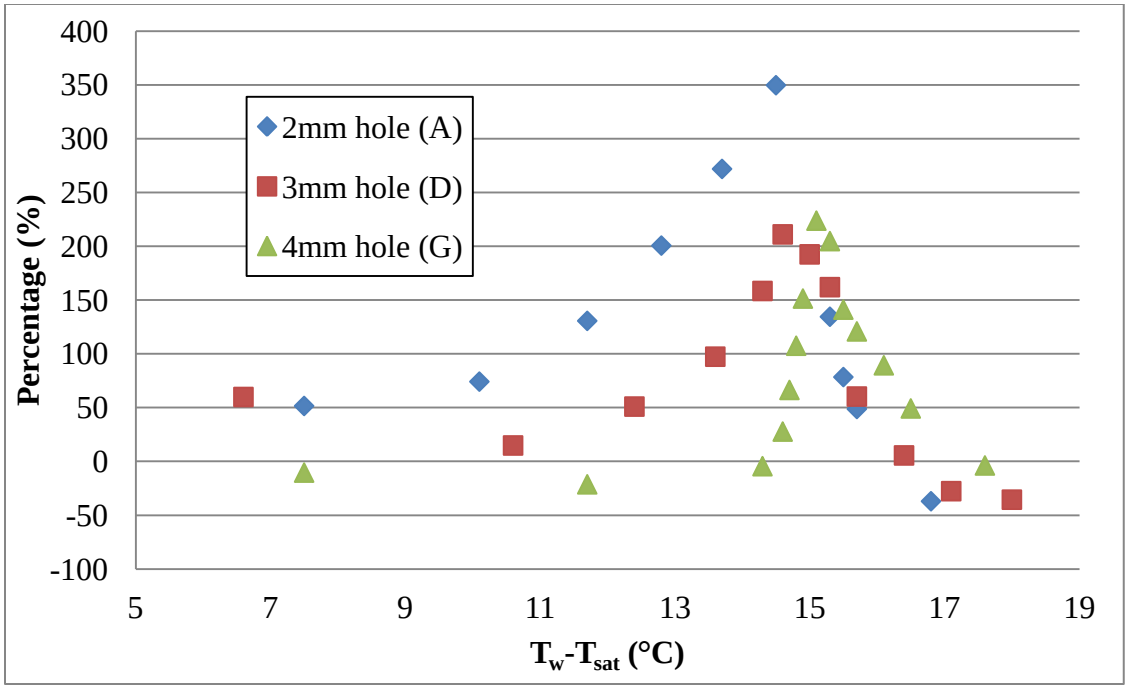

Figure 4.14 Percentage of enhancement in heat transfer coefficient as function of superheat (ΔT), case A, D and G

4.3.1 Analysis of pool boiling heat transfer performance by fluid and bubble behavior in confined spaces

From the Figure 4.13, it is evident that the maximum enhancement in heat transfer coefficient occurs at the ONB for the confined space in cases A and D, but no enhancement was observed in case G. Furthermore, the enhancement in case A is greater than that in case D. One possible explanation for the enhancement at ONB is that the single phase liquid experiences a significant radial temperature rise in the direction of the hole as seen in Figure 4.15, which suggests the formation and development of radial flow in higher temperature along the surface. The apparent hotter radial flow of single phase liquid helps increase nucleation and growth of fresh bubbles, which in turn helps

in the detachment of small bubbles. Most of the results indicate that at ONB, heat transfer performance is enhanced by decreasing the hole diameter on the plate.

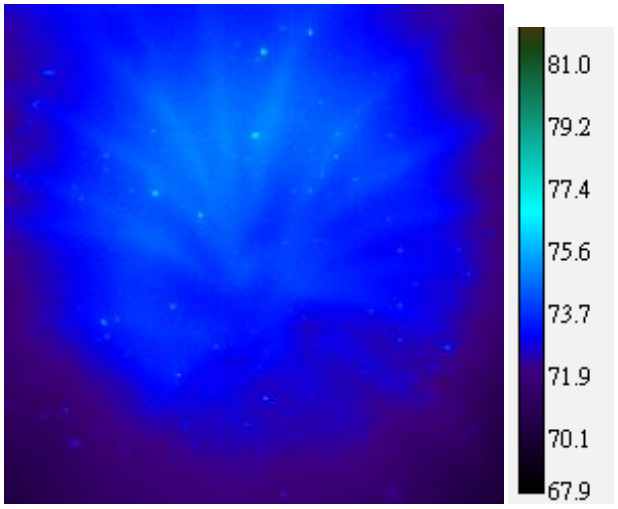

Figure 4.15 IR image of surface temperature field caused by the motion of fluid in the confined space for case D at a heat flux of 1.5 W/cm^2

The effect of gap size on enhanced pool boiling performance can be observed in Figures 4.4 through 4.6 and briefly described in Table 4.2. In summary, a small hole size results in better heat transfer performance in the low heat flux region, while a larger hole size exhibits better performance in the high heat flux region. In both cases, the effect of large bubble coalescence of bubble seems to be the determining factor that influences the heat transfer performance. Figures 4.16 and 4.17 show the effect of hole diameter on the bubble coalescence.

		Bubble images
2 mm hole (A)	Top view	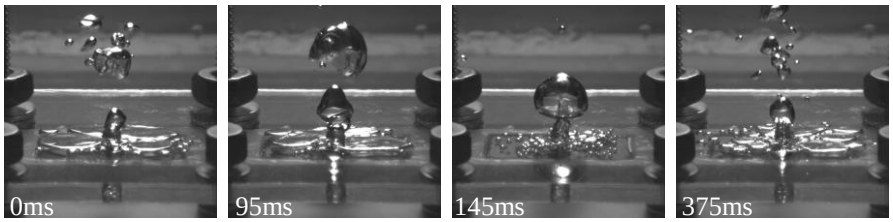
3 mm hole (D)	Top view	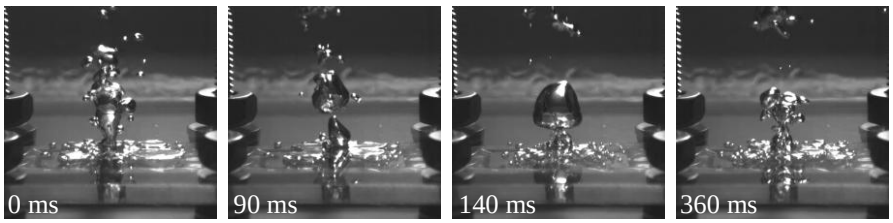
4 mm hole (G)	Top view	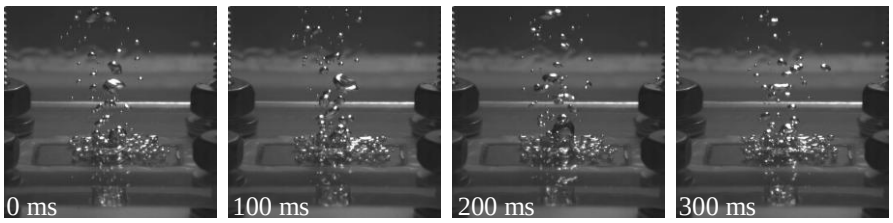

Figure 4.16 Bubble image of confined space in 2.3 mm gap with different hole diameter, 4.2 W/cm^2

		Bubble image
4 mm hole (G)	Top view	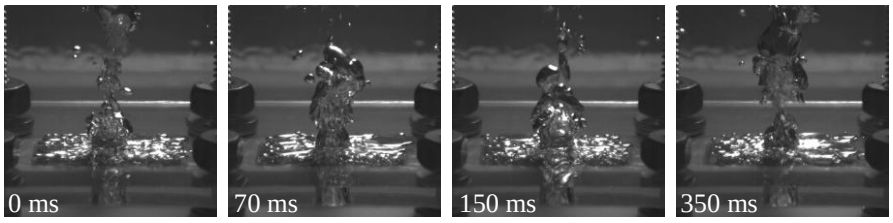

Figure 4.17 Bubble image of confined space in 2.3 mm gap with 4 mm hole diameter, 17W/cm^2

From the bubble images shown in Figure 4.16, it can be observed that the smaller hole size (2 mm) leads to the formation and frequent departure of coalesced bubbles

(case A). However, with the hole diameter increases, the effect of confinement decreases, which leads to the decrease of bubble coalescence. In fact, less coalesced bubbles are observed in case D, and no coalesced bubble can be seen in case G, which is characterized by having the worst heat transfer performance when the gap size is 2.3 mm. There are two explanations of how the coalesced bubbles affect heat transfer performance in confined spaces at the low heat flux. First, the coalesced bubble in the narrow confined space should absorb small bubbles formed on the surface which in turn accelerate their departure [36]. Second, when the coalesced bubble moves in the confined space, the sweeping effect should improve the vaporization of the liquid film between the coalesced bubble and surface [31]. Furthermore, the shear flow caused by the departure of coalesced bubble which is discussed in section 4.2 also should improve the departure of small bubbles from the surface.

On the other hand, when heat flux is increased as seen in Figure 4.17, it leads to heat transfer enhancement due to a significant occurrence of bubble coalescence. Furthermore, bubbles tend to coalesce at a higher rate at high heat flux than at low heat flux. However, when the hole size is decreased, heat transfer performance worsens because the phenomenon of dryout, which is discussed in section 4.2.

4.3.2 Analysis of pool boiling heat transfer performance due to coalesced bubble departure frequency and diameter

This section discusses the effect of hole diameter on heat transfer performance by measuring the departure frequency and diameter of coalesced bubbles. In order to obtain

the departure frequency and the diameter of coalesced bubbles, high speed camera images of bubble were used. The departure frequency was measured by counting the number of coalesced bubble departing from the hole every two seconds. In the measurement of coalesced bubble diameter, it was assumed that the departure bubble was always spherical. The diameter of each bubble was measured and the average diameter of coalesced bubbles was obtained by averaging the diameter of ten coalesced bubbles.

Coalesced bubble frequency and diameter were only measured using observations made in Cases A and D since they exhibited continuous bubble coalescence. Table 4.3 shows the effects of heat flux on coalesced bubble frequency and diameter. Figures 4.18 and 4.19 show the departure frequency and diameter of coalesced bubble in cases A and D. It can be also observed that the departure diameter of coalesced bubble increases with heat flux; however, the departure frequency initially increases until it reaches a limit. From Figure 4.19, it is evident that maximum bubble diameter depends on hole size.

Heat flux (W/cm^2)	Frequency (Hz)		Diameter (mm)	
	2 mm hole	3 mm hole	2 mm hole	3 mm hole
3	20	13.3	3.5	3.7
4.3	25	19	3.9	4
7.8	28	23	5.3	5.6
10	27	25.5	5.9	6.6
12.5	x	26	x	7.1
15	x	24.5	x	7.7

Table 4.3 Departure frequency and diameter of confined space with 2 mm and 3 mm hole in the different value of heat flux

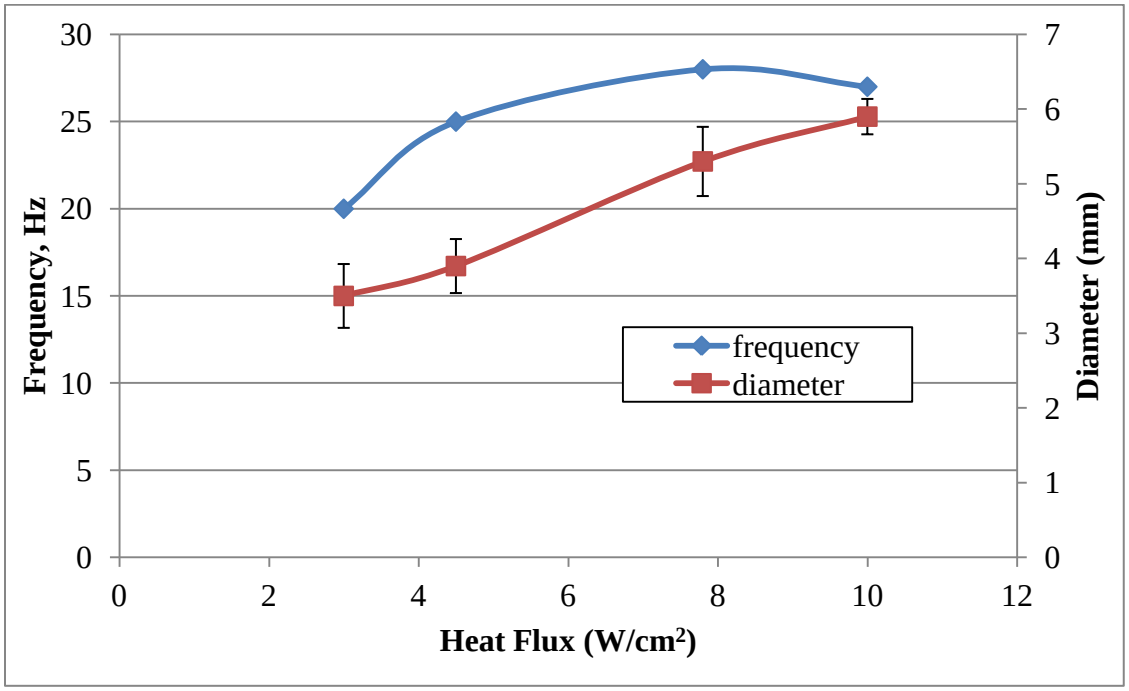

Figure 4.18 Departure frequency and diameter of the coalesced bubble as a function of heat flux in the confined space with 2 mm hole (case A)

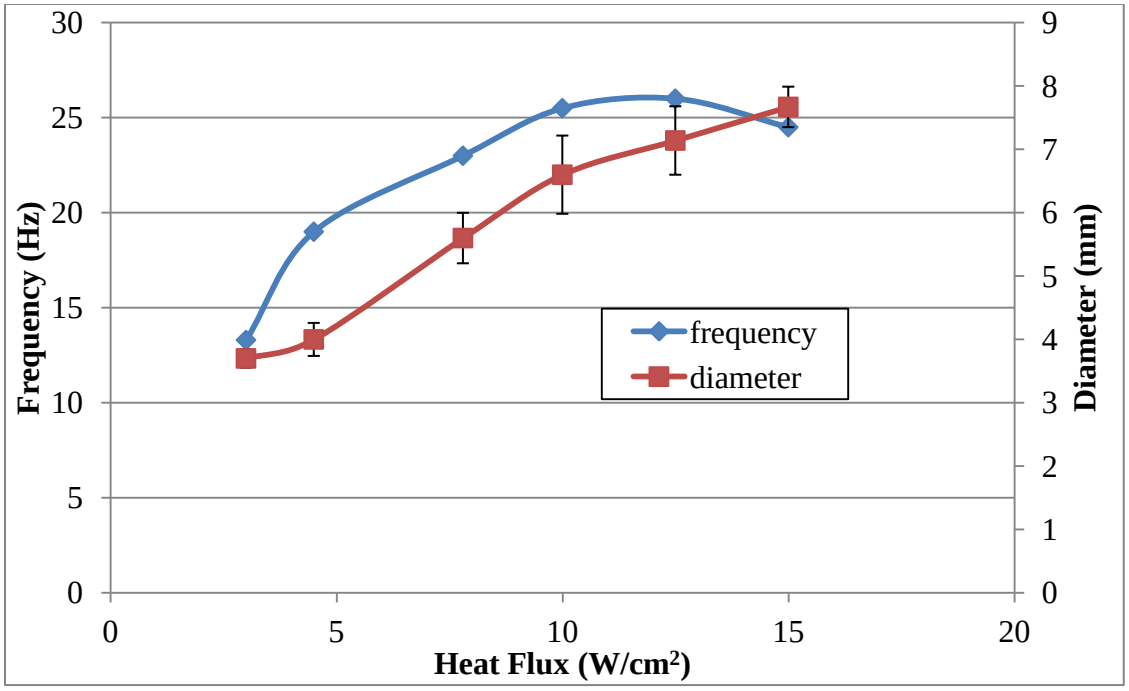

Figure 4.19 Departure frequency and diameter of the coalesced bubble as a function of heat flux in the confined space with 3 mm hole (case D)

The effect of superheat (T_w-T_{sat}) on coalesced bubble departure frequency and diameter is shown in Table 4.4. Figures 4.20 and 4.21 show the effect of superheat on coalesced bubble departure frequency and diameter for two hole sizes. It is evident that smaller hole size can induce a choking effect that limits bubble departure frequency. This suggests that hole diameter should be chosen carefully to ensure adequate bubble dynamics.

T_w-T_{sat} (°C)	Frequency (Hz)		Diameter (mm)	
	2 mm hole	3 mm hole	2 mm hole	3 mm hole
13.6	26	13.3	4.8	3.7
14.5	28	21	5.3	4.6
15.3	30	25.5	5.5	6.6
15.7	25.5	26	6.1	7.1

Table 4.4 Departure frequency and diameter of coalesced bubble in confined space with 2 mm and 3 mm hole

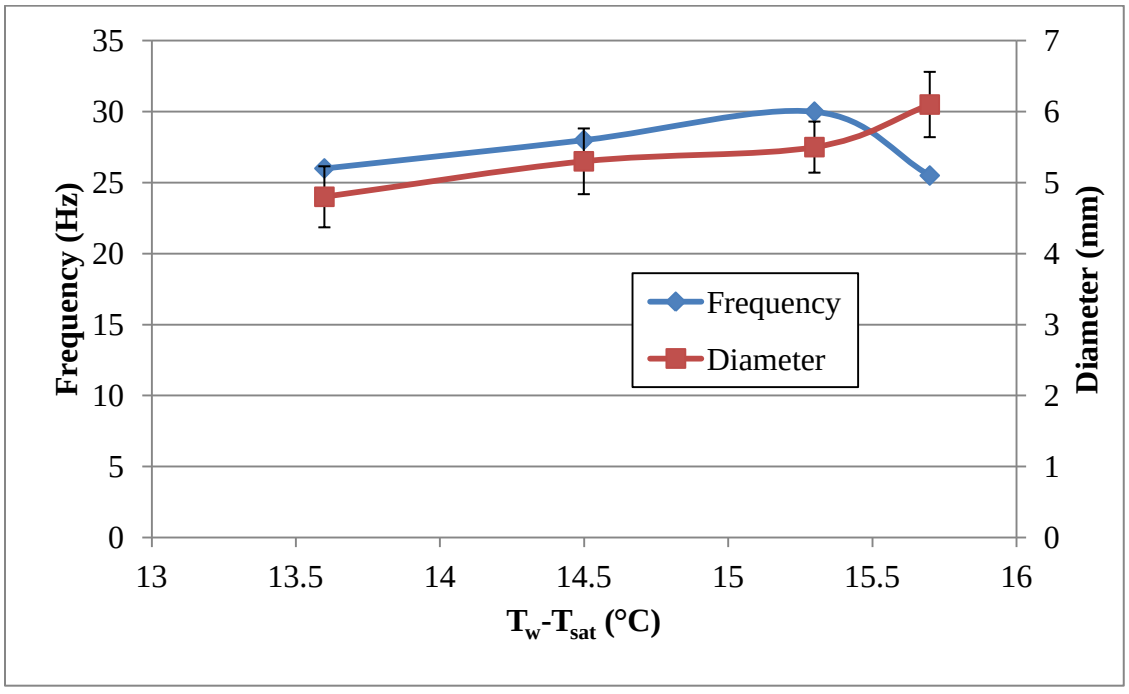

Figure 4.20 Departure frequency and diameter of the coalesced bubble as a function of ΔT in the confined space with 2 mm hole (case A)

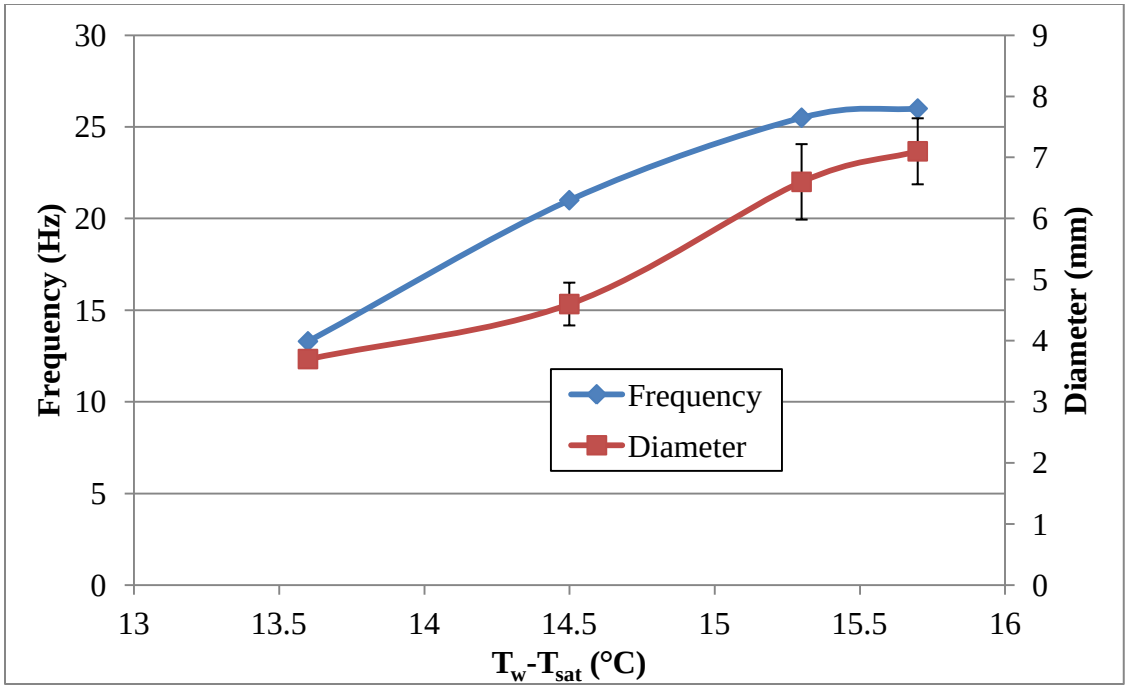

Figure 4.21 Departure frequency and diameter of the coalesced bubble as a function of ΔT in the confined space with 3 mm hole (case D)

In order to investigate the influence of diameter and frequency on confined space pool boiling, the value of frequency times volume of departure bubble $(f \cdot V)$ or bubble volume flow rate was calculated based on the assumption that coalesced bubbles are always spherical and that small bubbles contribute little in terms of volume flow rate. Figures 4.22 and 4.23 show the effects of heat flux and superheat on bubble volume flow rate, respectively. The amount of bubble volume flow rate is a direct measure of the amount of liquid being drawn into the confined space when the coalesced bubbles depart. Furthermore, the space left behind by the coalesced bubble results in the formation of intermittent shear flow within the confined space. Therefore, greater value of $f \cdot V$ leads to cooler liquid drawn into the confined space which leads to better heat transfer

performance under identical low heat flux conditions as shown in Figure 4.13. From Figures 4.22 and 4.23, the trend of $f \cdot V$ correlates well with the trend of percentage of enhancement as shown in Figures 4.13 and 4.14, which supports the notion that greater $f \cdot V$ results in better heat transfer performance. From Figure 4.23, it can be inferred that the 2-mm hole outperforms the 3-mm hole at superheat values are below 15 ℃. From Figure 4.14, it is evident that the rate of bubble nucleation and bubble departure rate from the surface leads to enhanced heat transfer performance because of the confined space ability to ensure high bubble flow rate at those superheat values.

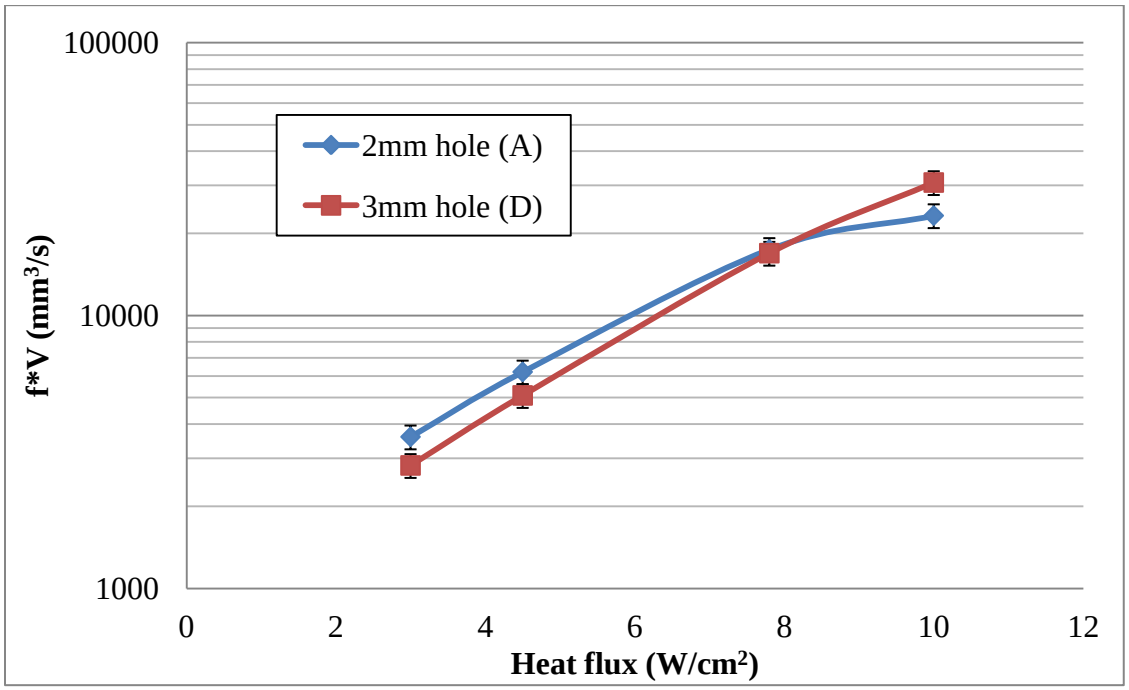

Figure 4.22 Comparison of the frequency times volume as a function of heat flux in the confined space with 2 mm and 3 mm hole

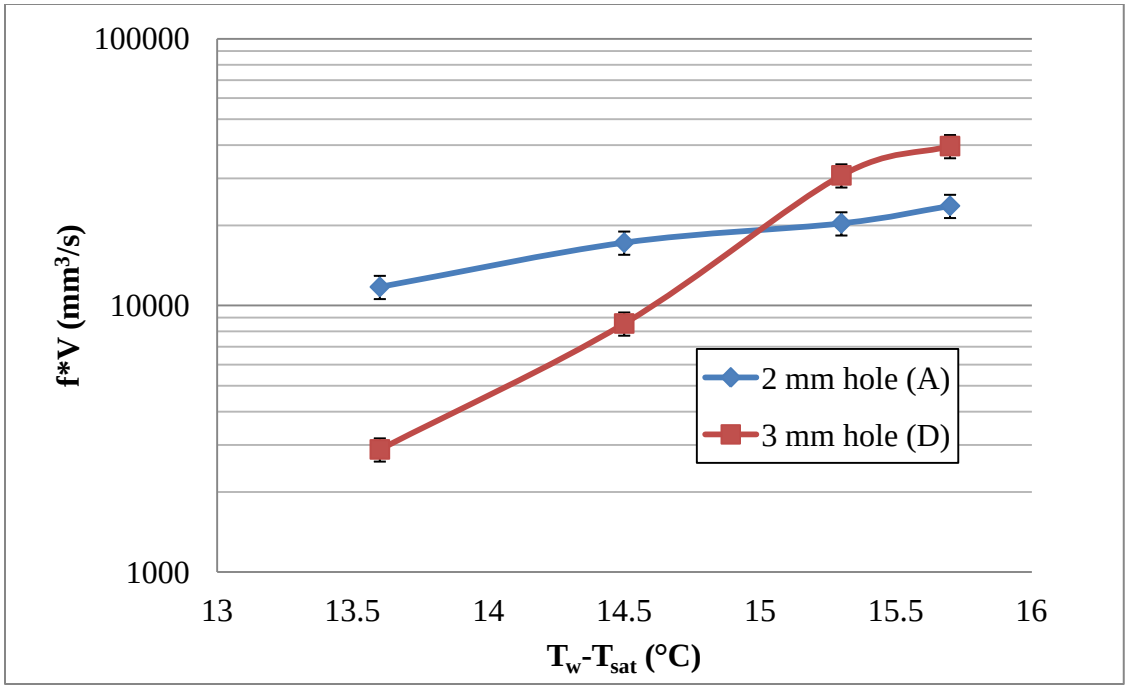

Figure 4.23 Comparison of the frequency times volume as a function of ΔT in the confined space with 2 mm and 3 mm hole

4.4 Effect of the triple hole plate on confined pool boiling

From the result shown in section 4.3, the confined space in the case A shows better heat transfer performance in the low heat flux region because bubble coalescence is prevalent. However, in higher heat flux region, there is no enhancement in the case of the 2 mm hole (case A) because the confined space experiences early dry out phenomena due to the confined space inability to allow high bubble flow rate as seen in Figure 4.22 at heat flux values over 10 W/cm^2. Therefore, in order to avoid early dryout in the confined space, more holes should be used to increase bubble flow rate and heat transfer.

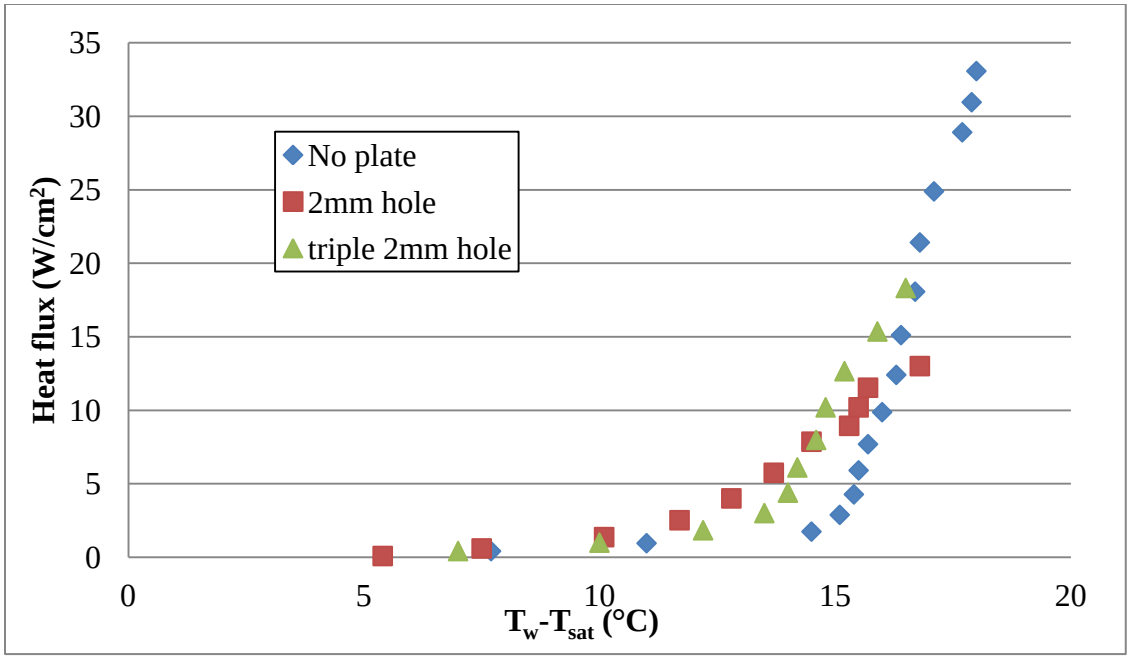

Figure 4.24 Boiling curve of the confined space with 2 mm hole and triple 2 mm holes and 2.3 mm gap

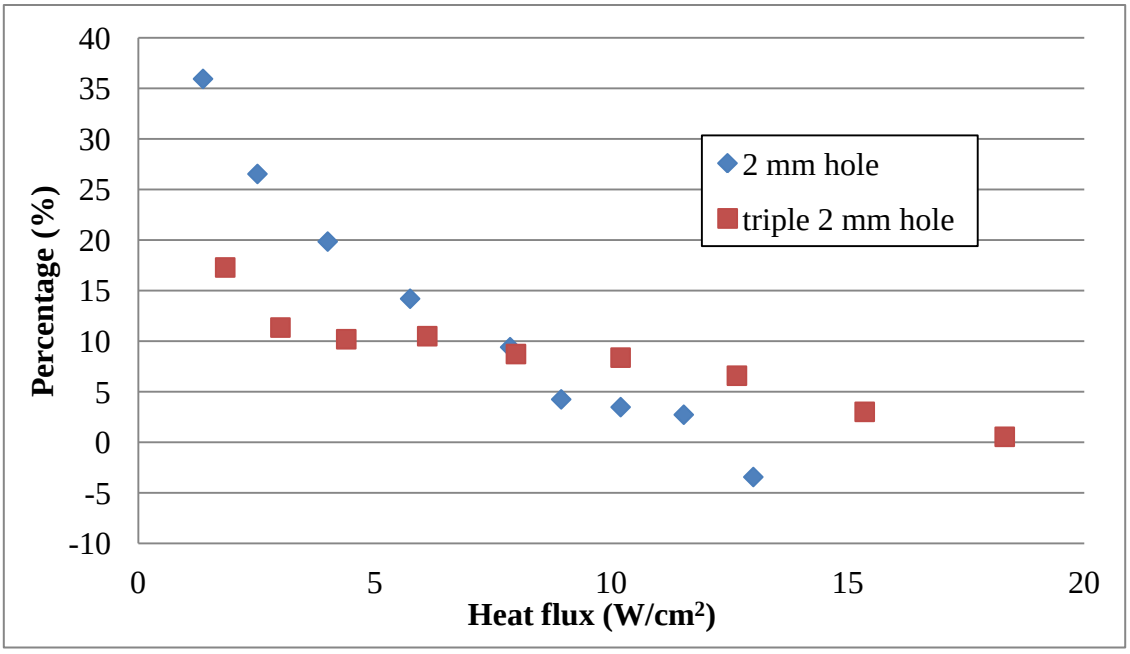

Figure 4.25 Percentage of enhancement in heat transfer coefficient as a function of heat flux

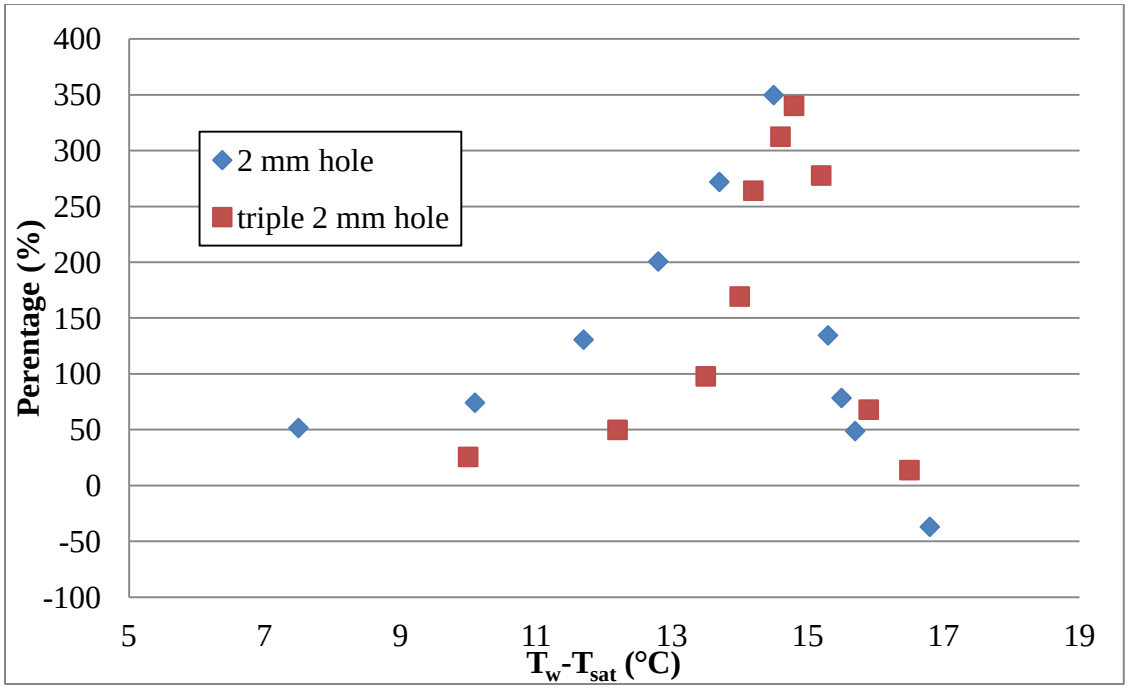

Figure 4.26 Percentage of enhancement in heat transfer coefficient as a function of superheat (ΔT)

Figure 4.24 shows the boiling curve in the confined space with a 2 mm hole (case A) and triple holes. As seen in Figure 4.24, the confined space with triple holes shows better heat transfer performance in the high heat flux region when compared to the confined case with a 2-mm hole and unconfined case. When a triple hole plate is used, a heat transfer enhancement of 17% at the ONB (1.5 W/cm^2) can be achieved as seen in Figure 4.25. On the other hand, as seen in Figure 4.26, it shows a significant enhancement in heat transfer when superheat (T_w-T_{sat}) is about 15 ℃, which is similar to the enhancement percentage seen in case A.

It can be observed that the confined space with triple hole results in better heat transfer performance in the higher heat flux region because of the greater amount of

coalesced bubbles that can depart easily from the confined space when more holes are present, as seen in Figure 4.27. However, the confined space with a single 2 mm hole still exhibits better heat transfer performance in the low heat flux region. This also can be explained by the bubble images as shown in Figure 4.28, which shows that having a single hole promotes better heat transfer performance than when three holes are present because bubble flow through the three holes tends to be more chaotic and random in nature. Furthermore, the occurrence of bubble coalescence diminishes when a triple hole plate is used, resulting in a weaker shear flow within the confined space. High speed images also revealed that the sweeping effect decreases when a triple hole plate is used. All of these factors combined suggest that a triple hole plate should be used only at relatively high superheat values.

		Bubble images
Triple 2 mm hole	Top view	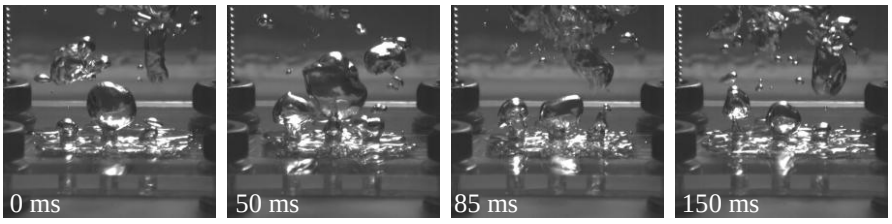

Figure 4.27 Bubble image of the confined space with triple 2 mm hole plate in 2.3 mm gap, 15 W/cm^2

		Bubble images
2 mm hole (A)	Top view	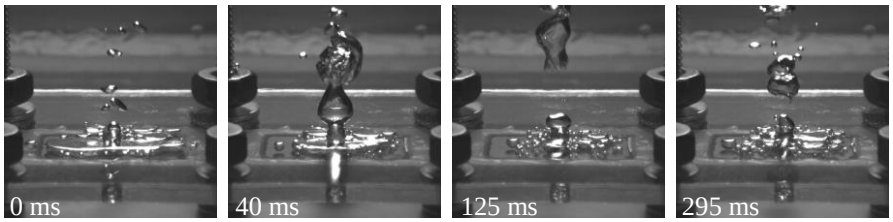
Triple 2 mm hole	Top view	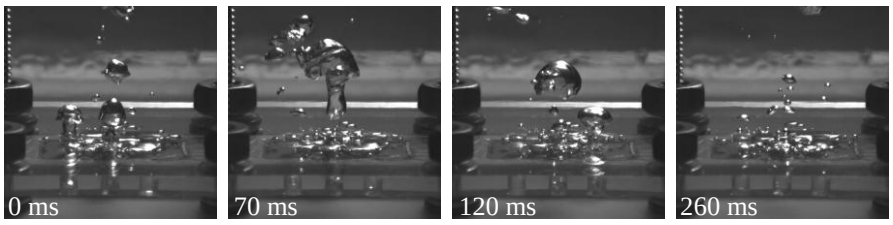

Figure 4.28 Bubble image of the confined space with 2 mm hole and triple 2 mm hole plate in 2.3 mm gap, 3 W/cm^2

5. CONCLUSION

The effect of confinement on pool boiling was studied by considering several system parameters. Bubble images and surface temperature distribution acquired using high speed and infrared camera imaging systems to understand the effects of space confinement parameters including hole diameter and gap size on pool boiling. Furthermore, heat transfer performance of pool boiling in the confined spaces using a triple 2 mm hole plate was also characterized and compared to that of a confined space with a single 2 mm hole.

From the results of all the cases with a single hole (Cases A – I), it was found that the confined space with the smallest gap size yields the best heat transfer performance. The enhancement can be attributed to the induced shear flow caused by the departure of coalesced bubbles through the plate hole. On the other hand, due to the reduction in the magnitude of shear flow in the cases of confined space with greater gap size, poorer heat transfer performances of pool boiling was observed.

The effect of hole diameter on pool boiling when the gap size was fixed at 2.3 mm was also investigated. The results indicate that the best heat transfer enhancement occurs when a 2 mm hole plate (case A) is used. The possible explanation for the enhancement especially at ONB could be caused by an increase in the rate of bubble nucleation and growth that result from the hotter radial flow of single phase liquid. On the other hand, the enhancement in the low heat flux region can be attributed to a significant level of bubble coalescence within the confined space. The coalesced bubble in the narrow confined space would absorb the smaller bubbles formed on surface,

which accelerate small bubble departure rate. In addition, when the coalesced bubble moves out the confined space, the sweeping effect would improve the vaporization of the liquid film between the coalesced bubble and surface. Furthermore, by measuring the departure frequency and diameter of coalesced bubbles, greater bubble volume flow rate $(f \cdot V)$ results in better heat transfer performance which supports the notion that fluid flow within the confined space enhances heat transfer.

From the result of triple 2 mm hole experiments, it was found that the heat transfer performance was better than in case A in the high heat flux region. However, case A still shows better enhancement of heat transfer performance in the low heat flux region. The better performance of case with triple hole in the high heat flux region can be attributed to easier departure of coalesced bubbles through the hole which inhibits the occurrence of dryout. On the other hand, in the low heat flux region, the better performance of case A still can be explained by significant bubble coalescence and the sweeping effect within the confined space.

In summary, pool boiling can be enhanced by confining the heat transfer area where bubble nucleation and bubble growth takes place and by taking advantage of naturally occurring buoyancy flows that could induce intermittent shear flow necessary for an increase in bubble detachment.

REFERENCES

[1] Nukiyama, S., *The maximum and minimum values of the heat Q transmitted from metal to boiling water under atmospheric pressure* Journal of Japan Society of Mechanical Engineers, 1934. **37**: p. 367-374.

[2] Carey, V.P., *Liquid-vapor phase-change phenomena*. 1992, Hemisphere, New York.

[3] Rohsenow, W.M., *A method of correlating heat transfer data for surface boiling liquids.* Transactions of ASME, 1953. **74**: p. 969-976.

[4] Forster, H.K. and G. R, *Heat transfer to a boiling liquid - mechanisms and correlations.* ASME Jounral of Heat Transfer, 1959. **81**: p. 45.

[5] Mikic, B.B. and W.M. Rohsenow, *A new correlation of pool boiling data including teh effect of heating surface characteristics.* ASME Jounral of Heat Transfer, 1969. **91**: p. 245.

[6] Bergles, A.E., *Enhancement of pool boiling.* International Journal of Refrigeration, 1997. **20**(8): p. 545-551.

[7] Berenson, P.J., *Experiments on pool-boiling heat transfer.* International Journal of Heat and Mass Transfer, 1962. **5**(10): p. 985-999.

[8] Bankoff, S.G., *The prediction of surface temperatures at incipient boiling.* Chem. Eng. Progress Symp. Ser., Heat Transfer, AIChE, 1959. **55**: p. 87-94.

[9] Grigor'ev, V.A., Y.M. Pavlov, and E.V. Ametistov, *Boiling of cryogenic fluids.* Energiya Publishing House, 1977: p. 289.

[10] Khan, N., D. Pinjala, and K.C. Toh, *Pool boiling heat transfer enhancement by surface modification / micro structures for electronics cooling: a review.* Electronics Packaging Technology Conference, 2004: p. 273-280.

[11] Takata, Y., et al., *Effect of surface wettability on boiling and evaporation.* Energy, 2005. **30**(2-4): p. 209-220.

[12] Lu, M.-C., et al., *Critical heat flux of pool boiling on Si nanowire array-coated surfaces.* International Journal of Heat and Mass Transfer, 2011. **54**(25-26): p. 5359-5367.

[13] Lienhard, J.H., V.K. Dhir, and D.M. Riherd, *Peak pool boiling heat-flux measurements on finite horizontal flat plates.* Journal of Heat Transfer, 1973. **95**: p. 477-482.

[14] Rainey, K.N. and S.M. YOU, *Effects of heater size and orientation on pool boiling heat transfer from microporous coated surfaces.* International Journal of Heat and Mass Transfer, 2001. **44**: p. 2589-2599.

[15] Park, K.A. and A.E. Bergles, *Effects of size of simulated microelectronic chips on boiling and critical heat flux.* Journal of Heat Transfer, 1988. **110**: p. 728-734.

[16] Cieśliński, J.T., *Nucleate pool boiling on porous metallic coatings.* Experimental Thermal and Fluid Science, 2002. **25**: p. 557-564.

[17] O'Connor, J.P., S.M. You, and D.C. Price, *A dielectric surface coating technique to enhance boiling heat transfer from high power microelectronics.* lEEE Transactions on Components, Packaging, and Manufacturing Technology-Part A, 1995. **18**(3).

[18] Vemuri, S. and K.J. Kim, *Pool boiling of saturated FC-72 on nano-porous surface.* International Communications in Heat and Mass Transfer, 2005. **32**(1-2): p. 27-31.

[19] Forrest, E., et al., *Augmentation of nucleate boiling heat transfer and critical heat flux using nanoparticle thin-film coatings.* International Journal of Heat and Mass Transfer, 2010. **53**(1-3): p. 58-67.

[20] Tang, Y., et al., *Pool-boiling enhancement by novel metallic nanoporous surface.* Experimental Thermal and Fluid Science, 2013. **44**: p. 194-198.

[21] Guglielmini, G., M. Misale, and C. Schenone, *Experiments on pool boiling of a dielectric fluid on extended surfaces.* International Communications in Heat and Mass Transfer, 1996. **23**(4): p. 451-462.

[22] Wei, J.J. and H. Honda, *Effects of fin geometry on boiling heat transfer from silicon chips with micro-pin-fins immersed in FC-72.* International Journal of Heat and Mass Transfer, 2003. **46**(21): p. 4059-4070.

[23] Cooke, D. and S.G. Kandlikar, *Effect of open microchannel geometry on pool boiling enhancement.* International Journal of Heat and Mass Transfer, 2012. **55**(4): p. 1004-1013.

[24] Jun, S., S. Sinha-Ray, and A.L. Yarin, *Pool boiling on nano-textured surfaces.* International Journal of Heat and Mass Transfer, 2013. **62**: p. 99-111.

[25] Fujita, Y. and Q. Bai, *Critical heat flux of binary mixtures in pool boiling and its correlation in terms of Marangoni number.* International Journal of Refrigeration, 1997. **20**(8): p. 616-622.

[26] Choi, S.U.S. and J.A. Eastman, *Enhancing thermal conductivity of fluids with nanoparticles.* ASME FED, 1995. **231**: p. 99-103.

[27] Bang, I.C. and S.H. Chang, *Boiling heat transfer performance and phenomena of Al2O3–water nano-fluids from a plain surface in a pool.* International Journal of Heat and Mass Transfer, 2005. **48**(12): p. 2407-2419.

[28] Tu, J.P., N. Dinh, and T. Theofanous, *An experimental study of nanofluid boiling heat transfer.* Proceedings of 6th International Symposium on Heat Transfer, Beijing, China, 2004.

[29] Wen, D. and Y. Ding, *Experimental investigation into the pool boiling heat transfer of aqueous based γ-alumina nanofluids.* Journal of Nanoparticle Research, 2005. **7**(2-3): p. 265-274.

[30] Kim, S.J., et al., *Surface wettability change during pool boiling of nanofluids and its effect on critical heat flux.* International Journal of Heat and Mass Transfer, 2007. **50**(19-20): p. 4105-4116.

[31] Nishikawa, K., et al., *Effect of heating surface orientation on nucleate boiling heat transfer.* Proc. ASME-JSME Thermal Engineering Joint Conference, 1983. **1**.

[32] Hsu, Y.Y., *On the size range of active nucleation cavities on a heating surface.* Journal of Heat Transfer, 1962. **84**: p. 207-213.

[33] Katto, Y., S. Yokoya, and K. Teraoka, *Nucleate and transition boiling in a narrow space between two horizontal, parallel disk-surfaces.* Bulletin of the Japan Society of Mechanical Engineers, 1977. **20**(143).

[34] Passos, J.C., et al., *Confined boiling of FC72 and FC87 on a downward facing heating copper disk.* International Journal of Heat and Fluid Flow, 2004. **25**(2): p. 313-319.

[35] Rops, C.M., et al., *Enhanced heat transfer in confined pool boiling.* International Journal of Heat and Fluid Flow, 2009. **30**(4): p. 751-760.

[36] Zhao, Y., T. Tsuruta, and C. Ji, *Experimental study of nucleate boiling heat transfer enhancement in a confined space.* Experimental Thermal and Fluid Science, 2003. **28**(1): p. 9-16.

[37] Hendricks, T.J., et al., *Enhancement of pool-boiling heat transfer using nanostructured surfaces on aluminum and copper.* International Journal of Heat and Mass Transfer, 2010. **53**(15-16): p. 3357-3365.

[38] Auracher, H. and W. Marquardt, *Heat transfer characteristics and mechanisms along entire boiling curves under steady-state and transient conditions.* International Journal of Heat and Fluid Flow, 2004. **25**(2): p. 223-242.

[39] Rainey, K.N., S.M. You, and S. Lee, *Effect of pressure, subcooling, and dissolved gas on pool boiling heat transfer from microporous, square pin-finned surfaces in FC-72.* International Journal of Heat and Mass Transfer, 2003. **46**: p. 23-35.

[40] Chang, J.Y. and S.M. You, *Boiling heat transfer phenomena from micro-porous and porous surfaces in saturated FC-72* International Journal of Heat and Mass Transfer, 1997. **40**(18): p. 4437-4447.

[41] Rini, D.P. and R.-H. Chen Lou, *Bubble Behavior and Heat Transfer Mechanism in Fc-72 Pool Boiling.* Experimental Heat Transfer, 2001. **14**(1): p. 27-44.

[42] Yu, C.K., D.C. Lu, and T.C. Cheng, *Pool boiling heat transfer on artificial micro-cavity surfaces in dielectric fluid FC-72.* Journal of Micromechanics and Microengineering, 2006. **16**(10): p. 2092-2099.

[43] Guglielmini, G., M. Misale, and C. Schenone, *Boiling of saturated FC-72 on square pin fin arrays.* International Journal of Thermal Sciences, 2002. **41**: p. 599-608.

[44] Yu, C.K. and D.C. Lu, *Pool boiling heat transfer on horizontal rectangular fin array in saturated FC-72.* International Journal of Heat and Mass Transfer, 2007. **50**(17-18): p. 3624-3637.

[45] El-Genk, M.S. and H. Bostanci, *Saturation boiling of HFE-7100 from a copper surface, simulating a microelectronic chip.* International Journal of Heat and Mass Transfer, 2003. **46**(10): p. 1841-1854.

[46] Misale, M., G. Guglielmini, and A. Priarone, *HFE-7100 pool boiling heat transfer and critical heat flux in inclined narrow spaces.* International Journal of Refrigeration, 2009. **32**(2): p. 235-245.

[47] El-Genk, M.S. and J.L. Parker, *Enhanced boiling of HFE-7100 dielectric liquid on porous graphite.* Energy Conversion and Management, 2005. **46**(15-16): p. 2455-2481.

APPENDIX A

UNCERTAINTY ANALYSIS

1. Emissivity measurement

The process of emissivity measurement has been introduced in Section 3.2.1. The equation used to calculate the emissivity is shown in Equation 1.

$$\varepsilon_{tgt} = \frac{D_{tgt} - D_{bkg}}{D_{ref} - D_{bkg}} \varepsilon_{ref} \tag{1}$$

By using the Kline-McClintock methodology as seen in section 3.2.4, the uncertainty of emissivity measurement can be estimated. The proposed expression of the emissivity uncertainty is expressed as follows:

$$\frac{\Delta \varepsilon_{tgt}}{\varepsilon_{tgt}} = \sqrt{\left(\frac{\Delta(D_{tgt} - D_{bkg})}{D_{tgt} - D_{bkg}}\right)^2 + \left(\frac{\Delta(D_{ref} - D_{bkg})}{D_{ref} - D_{bkg}}\right)^2 + \left(\frac{\Delta \varepsilon_{ref}}{\varepsilon_{ref}}\right)^2} \tag{2}$$

The reference used in the IR measurement was an electrical vinyl tape Super 88 with a known emissivity value of $\varepsilon_{ref} = 0.95 \pm 0.05$. The uncertainty of the count reading was found by computing the standard deviation of count reading of the reference and target. It was assumed that the count reading data acquired by IR camera follows a normal distribution. A range of three times standard deviation gives a probability of 99.7% that the results fall within the range of accuracy. By applying Equation 2, the uncertainty of emissivity is about 5.2% (0.4±0.021).

2. Heat flux measurement

Heat flux value was calculated from Equation 3, which is presented in Section 3.2.3.

$$q'' = \frac{P_{in} - Q_{loss}}{A} \tag{3}$$

It is noted that the heat loss (Q_{loss}) is a function of surface temperature as expressed by Equation 4, which has been included in Section 3.2.2.

$$Q_{loss} = 0.083T_{difference} + 0.0067 \tag{4}$$

By substituting Equation 4 into Equation 3, and the expression of heat flux value uncertainty is as follows.

$$\frac{\Delta q''}{q''} = \sqrt{\left(\frac{\Delta V}{V}\right)^2 + \left(\frac{\Delta I}{I}\right)^2 + 0.083\left(\frac{\Delta T}{T}\right)^2 + \left(\frac{\Delta A}{A}\right)} \tag{5}$$

The error associated with the measurement of voltage and current of power supply were obtained from the equipment specifications as posted by manufacturers as follows:

Error in voltage = 0.1% reading + 0.2% rated output voltage

Error in current = 0.1% reading + 0.4% rated output current

The uncertainty of surface temperature was also acquired by taking into account the standard deviation and the assumption that the temperature map also

follows of normal distribution when uniform heat flux is applied. The uncertainty of heat flux value is about 2%.

3. Enhancement percentage in heat transfer coefficient

The heat transfer coefficient was calculated from Equation (6), and the enhancement percentage in heat transfer coefficient was calculated from Equation (7), which is presented in Section 4.3.

$$h = \frac{q''}{\Delta T} \tag{6}$$

$$\text{enhancement } \% = \frac{(h_{confined} - h_{unconfined})}{h_{unconfined}} \times 100\% \tag{7}$$

Therefore, the expression of heat transfer coefficient and the enhancement percentage uncertainty are as follows.

$$\frac{\Delta h}{h} = \sqrt{\left(\frac{\Delta q''}{q''}\right)^2 + \left(\frac{\Delta T}{T}\right)^2} \tag{8}$$

$$\frac{\Delta \text{enhancement } \%}{\text{enhancement } \%} = \sqrt{\left(\frac{\Delta h_{confined}}{h_{confined}}\right)^2 + \left(\frac{\Delta h_{unconfined}}{h_{unconfined}}\right)^2} \tag{9}$$

The uncertainty of heat transfer coefficient is about 3.6%, and the uncertainty of enhancement percentage is about 5%.

APPENDIX B

The following table depicts the required superheat (T_w-T_{sat}) for ONB and found in previous studies that used similar dielectric fluids as used in this study.

Fluid	**Material**	**Dimension**	**T_w-T_{sat} at ONB**	**Ref**
FC72	copper	10 mm × 10 mm	4 ℃	[39]
FC72	copper	10 mm × 10 mm	12 ℃	[40]
FC72	diamond plate	9 mm × 9 mm	10 ℃	[41]
FC72	silicon wafer	10 mm × 10 mm	5 ℃	[42]
FC72	smooth silicon	10 mm × 10 mm	20 ℃	[22]
FC72	copper	30 mm diameter	8 ℃	[43]
FC72	copper	10 mm × 10 mm	5 ℃	[44]
HFE-7100	copper	10 mm × 10 mm	14 ℃	[45]
HFE-7100	copper	7.07 cm^2	7 ℃	[46]
HFE-7100	graphite	10 mm × 10 mm	10 ℃	[47]

APPENDIX C

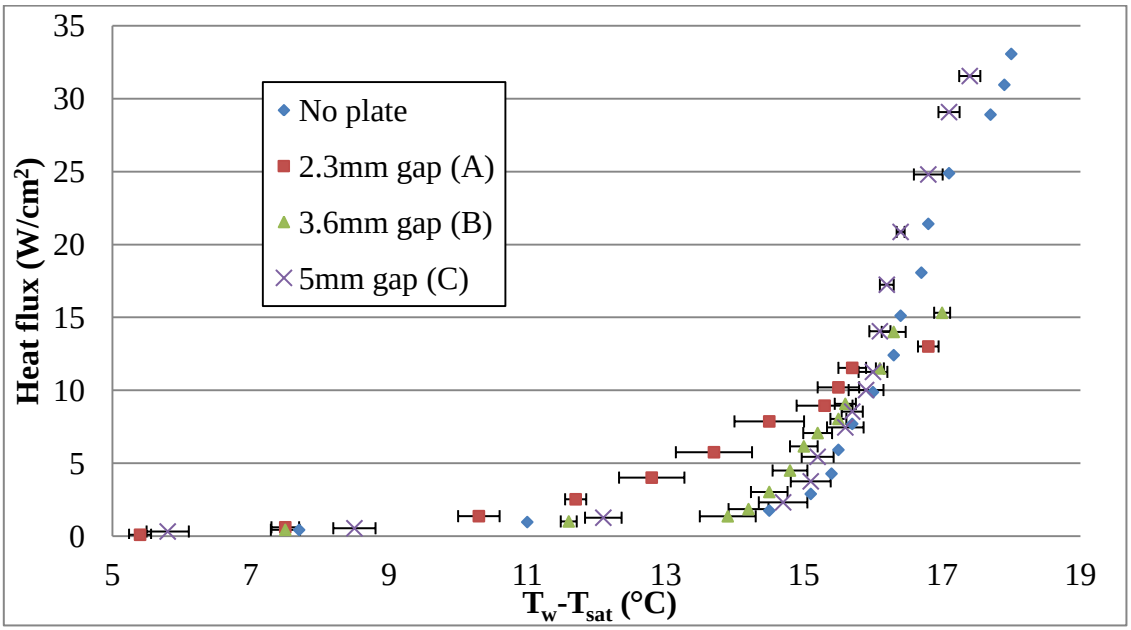

Figure C.1 Boiling curve with error bar of confined space with 2 mm hole plate, Case A – C

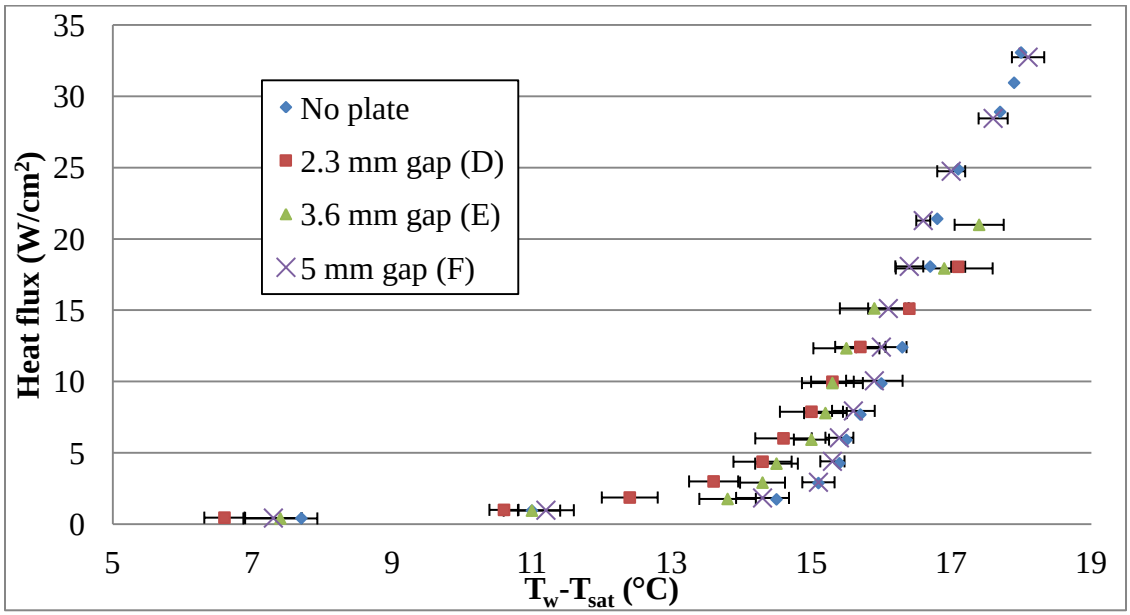

Figure C.2 Boiling curve with error bar of confined space with 3 mm hole plate, Case D – F